SOME WALL INTERFERENCE EFFECTS FOR FLOW PAST TRIANGULAR PRISMS

Nagy N. Sourial

MAJOR TECHNICAL REPORT

IN THE

FACULTY OF ENGINEERING

Presented in partial fulfilment of the requirements for

the degree of MASTER OF ENGINEERING

at

Sir George Williams University

Montreal, Canada.

April 1974

ABSTRACT

Nagy N. Sourial

SOME WALL INTERFERENCE EFFECTS
FOR FLOW PAST TRIANGULAR PRISMS

The object of the present project was to determine the effects of end gap on the vortex shedding frequency of symmetric equiangular prisms. The study also includes the reinterpretation of some results of eccentrically mounted bluff bodies conducted by earlier investigators.

ACKNOWLEDGEMENT

The author wishes to thank Dr. A. S. Ramamurthy for suggesting the subject for the research project. Part of the equipment was procured with funds made available through NRC Grant No. A6708.

TABLE OF CONTENTS

LIST OF TABLES

LIST OF FIGURES

Chapter 1

INTRODUCTION

General Remarks: Vortex shedding is an important factor in the design of structural elements subjects to flow induced vibrations. Several reviews on the topic of flow induced vibration caused by vortex shedding have appeared recently (1, 2, 3, 4, 5 and 6). Although considerable information exists about vortex shedding by bluff body models mounted centrally in a test section, the effects of end gap (Fig. 1) on the vortex shedding of bluff bodies have not been studied in detail. Information existing in this regard is limited to the data of Shaw (7), whose tests were conducted in a towing tank. Shaw's tests included the effects of end gap on the vortex shedding frequency on bluff cylinders and plates.

The eccentrically located body can be viewed as though it formed part of a multiple body configuration shown in Fig. 1(d). The latter is often termed as a partial row configuration. This interpretation is possible since a stream line can be replaced by a solid boundary.

Scope of the present project: The object of the present project was to determine the effects of end gap on the vortex shedding frequency of symmetric equiangular prisms (Fig. 2). The study also includes the reinterpretation of the results of eccentrically mounted bluff bodies conducted by earlier investigators (7, 8).

Chapter - 2

EXPERIMENTAL SET UP AND PROCEDURE

The tests were carried out in a 14" x 10" test section of a wind tunnel (Figs. 3, 4 and 5). The symmetric equiangular prisms were chosen as the basic shape for the tests. These models were made out of brass. They were 10 inches high and 0.85 inch wide. The outside surfaces were machined to a smooth finish.

The test body was held rigid in the tunnel test section to avoid model vibration. The body could be moved from the tunnel's center-line towards the side wall to provide various offsets from the center-line. These body locations determine the effect of eccentric mounting on the vortex shedding frequency. The vortex shedding frequency was detected in the early wake of the body with the help of the DISA hot film probe (Fig. 5).

The frequency of vortex shedding was obtained by recording the hot film signals on a strip chart. The signals were stored on a tape recorder and later analyzed with the help of the B & K wave analyzer-level recorder unit (Fig. 6). The instrumentation signal conditioning circuitry is shown in Figure 7.

The sampling time for data recording on the tape was 15 minutes for each run. This time was found to be sufficient for analyzing the recorded vortex shedding frequency data on the wave analyzer.

Other experimental procedures consisted of recording the velocity at the entrance to the test section with the help of a pitot tube - inclined manometer combination which in turn yielded the undisturbed (mean) velocity u at the plane of the test body (Fig. 5).

A simple computer program has been prepared for calculating the mean velocity u of the air at the test section for different room pressures and temperatures. Care was taken to center and align the model axis with the test section center-line. Checking of the zero reading of the inclined manometer was made before each run.

When the body was next to the wall it was sealed with a tape to avoid leakage. Low velocity flow in the test section was obtained by adjusting the bypass opening of the supply duct.

Chapter - 3

ANALYSIS OF RESULTS

Velocity Scale: Figures 8 and 9 indicate the results of present tests related to the vortex shedding frequency of prisms. Tables 1 to 6 provide additional information about the raw data and reduced data for flow past the prisms subject to wall interference. The various definitions related to data reduction are mentioned briefly in Appendix 1. Figures 13 and 14 show the strip chart records related to the hot film signals for a few selected body locations. Figures 15 and 16 denote the spectral density plots of recorded data.

Ng (9) used the gap velocity u, and the contracted jet velocity u_j (Fig. 1a) as the scaling factors for the modified steady force coefficients and the Strouhal numbers for the triangular prisms. For eccentrically located bluff body models, Lee (8) has shown that the approaching flow gets deflected towards the wider gap side when the dimensionless gap distance G/b is small. Consequently, the use of u, and u_j to denote the velocity scales for normalising the fluid forces and the vortex shedding frequencies may not be very appropriate here. Note that the value of C_D for eccentrically mounted bodies is reduced when the end gap is reduced (8).

Vortex shedding frequency - eccentrically mounted prisms: The basic vortex shedding frequency f was normalized using the lateral dimension b of the triangular body for the length scale and the undisturbed velocity u for the velocity scale. The resulting Strouhal numbers S for different end gaps of triangular prisms are tabulated as functions of Reynolds number R (Tables 5 and 6).

Although there was a change in the Strouhal number with variations in the end gap, no significant Reynolds number effects were observed. This behaviour is to be expected as the separation points for the prisms are fixed, and no boundary layer transition effects were apparent as in the case of circular cylinders (Fig. 10). As such, Strouhal number variation with end gaps for both the prisms have been replotted as functions of end gap for only one Reynolds number. In Figures 8 and 9 the results of Shaw related to the effect of end gap on the vortex shedding frequencies of normal plates and bluff cylinders are also included for comparison. The end gap appears to increase the Strouhal number gradually as the former is reduced. This is true for both orientations of the prisms tested ($\Theta = 0^{\circ}$ and $\Theta = 60^{\circ}$). The maximum value of the Strouhal number is attained when the gap G/b is of the order of 1.

Note that the value of the Strouhal number for zero gap (wall mounted body) is higher than that of the centrally mounted bluff body (e/b = 0), although the value of the Strouhal number at the former location is still lower than the peak value which was seen to occur at $G/b \simeq 1$. This trend seems to be quite distinct for all the bluff shapes shown in Figures 8 and 9 where in Shaw's data for other shapes are included for comparison.

Drag coefficients for eccentric locations: Table 1 indicates the reinterpreted results related to drag coefficients of a few bluff bodies located eccentrically in the test section reported by Ng (9) and Lee (8). Although for these results, the blockage factor (See

Appendix 1) is not the same as ir the present case, qualitative statements can be made about the general functional relationship between C_D and G/b.

Figure 11 indicates that the wall mounted prisms have the lowest drag coefficients. However, the value of C_D increases as the gap width is increased and reaches a maximum value of C_D when G/b is of the order of 1. In general, the interference effects of the side wall seem to be limited to gap widths of 1. However, for the case of the circular cylinder for which the separation point is not fixed, this kind of functional relationship between C_D and G/b could not be traced as Reynolds number effects (Fig. 12) are predominant for flow past a circular cylinder.

It is a little puzzling to see an increase in both C_D and S as the bodies are moved away from the wall (increasing gap width) in the range of $0 \leqslant G/b \leqslant 1$. This contrasts with the variations of Strouhal number and drag coefficient with Reynolds number for a circular cylinder mentioned earlier (Fig. 10). Based on tests related to visual observations (10), an explanation is advanced as follows. Consider the centrally mounted prism set at Θ° to the approaching flow. As the body is moved towards the wall the reduction in the end gap causes the flow to get deflected. Consequently the effective orientation of the prism is no longer Θ° and as such, the length scale to be chosen for normalising the fluid forces or the vortex shedding frequency ought to be much less than b. Consequently, one gets a lower value of C_D if the conventional definition of C_D is maintained for the deflected flows.

For similar reasons, one should expect an increase in the value of the Strouhal number S if the conventional definition of S is used for gaps which are significantly small ($G/b \simeq 1$). However, when the gap is very much less than unity ($G/b \ll 1$), the flow characteristics of such a configuration can be viewed as being similar to partial row configurations (Fig. 1 d). Here the flow through the narrow slit between the wall and the model edge constitutes a type of bleed flow. Consequently, one should expect a drastic change in the dynamic characteristics of the flow. In fact, when the body is mounted on the wall, the wall behaves as a splitter plate. The splitter plate can induce large changes in the vortex shedding frequency of bluff bodies (7).

Chapter - 4

CONCLUSION AND SCOPE FOR FURTHER WORK

CONCLUSION

The following conclusions are advanced, based on the test results and the reinterpretation of earlier data.

1. When the centrally mounted triangular prisms ($\Theta = 0^{\circ}$ and $\Theta = 60^{\circ}$) are moved towards the wall, the value of drag decreases continuously and reaches a minimum value at the zero gap location. The drag coefficient does not seem to get affected for values of G/b greater than 1.

2. The value of the Strouhal number increases as the body is moved towards the wall and reaches a maximum when the gap width G/b is of the order of 1. Its value drops slightly when the gap is further reduced.

3. The deflection of the approaching flow is in part responsible for the variations of the drag coefficient and the Strouhal number for eccentrically mounted prisms.

4. End gap effects may appear in different forms in field structures, for instance, the interference effects may lead to major modifications of the load pattern on an existing building due to the erection of an adjacent building.

SCOPE FOR FURTHER WORK

1. Detailed examination of smoke tunnel test should be conducted to determine qualitatively the values of flow deflection for various model configurations.

2. Closely spaced partial row model configuration tests should be conducted to establish the hypothesis that single models with very narrow gaps do in fact behave like the former configurations.

APPENDIX 1

List of symbols:

Symbol	Description
R	Reynolds number
S	Strouhal number normalised by u
u	The mean undisturbed velocity at the center-line of model location
Θ	Orientation of the body (prism)
ρ	Density of fluid (air)
ν	Kinematic viscosity of fluid (air)
b	Side of the equilateral triangular prism for (all $\Theta = 0^{o}$, $\Theta = 60^{o}$, fig. 2)
G	Gap width (fig. 1)
B	Test section width
b/B	Blockage (wall constraint)
C_D	Drag coefficient
d	Diameter of circular cylinder
f	Frequency of vortex shedding

Some definitions:

Blockage: The ratio of lateral model dimension (d for circles and b for the prisms) to the tunnel width B.

Reynolds number: For circles, $R = ud/\nu$

For triangles, $R = ub/\nu$

Drag coefficient: C_D = steady drag force/$\frac{1}{2}\rho u^2 A$

where,

ρ = the density of air,

A = area of any one of the bluff bodies

Strouhal number: $S = fb/u$, $S = fd/u$

where,

f - frequency

u - velocity at separation

BIBLIOGRAPHY

1. Marris, A. W.: "A Review on Vortex Streets Periodic Wakes and Induced Vibration Phenomena", Paper No. 62-WA-106-ASME, 1963.

2. Naudascher, E.: "On the Role of Eddies in Flow Induced Vibrations", - Proc. of the 10th Congress - Vol. 3, 1963.

3. Scrutton, C.: "On the Wind Excited Oscillations of Towers and Masts", - International Conference on Wind Effects on Bridges and Structures - N. P. L. Teddington-England, 1963.

4. Morkovin, M. V.: "Flow Around Circular Cylinder - A Kaleidoscope of Challenging Fluid Phenomena", - Symposium on fully separated flows - Fluids Engineering Division - ASME, 1964.

5. Jaeger, C.: "Vibration and Resonance in Large Hydropower Systems", - Proc. 10th Congress of International Association of Hydraulic Research, 1963.

6. Toebes, G. H.: "Flow Induced Structural Vibrations", - J. Engg. Mech. Div. - ASCE - Vol. 91, Dec. 1965.

7. Shaw, T. L.: "Wake Dynamics of Two Dimensional Structures in Confined Flows", - Proc. of the 14th Congress of International Association of Hydraulic Research - Vol. 2, pp. 41-48, Paris, 1971.

8. Lee, P. M.: "Boundary Effects on Flow Past Bluff Bodies", D. Eng. Thesis, Sir George Williams University, Montreal, 1973.

9. Ng, C. P.: "Wall Interference Effects on Steady Force Coefficients of Bluff Bodies", M. Eng. Thesis, Sir George Williams University, Montreal, 1972.

10. Ramamurthy, A. S. and Subramanya, K.: "Interpretations of Interference Effects for Flow Past Bluff Bodies" - Sent for publication, 1974.

11. Toebes, G. H. and Ramamurthy, A. S.: "Energy Transfer Characteristics of Triangular Cylinders" - ASCE Structural Engineering Meeting, Louisville, Ky., April 1969.

Table 1 - DRAG COEFFICIENTS FOR ECCENTRIC LOCATIONS OF BLUFF BODIES (Ref. 7 and 9)

b/B Blockage (b, d, inch)	G/b Gap Width*	e/b Eccentricity	R Rey. No. x 10^{-4}	C_D	Shape and Configuration
.324	0.00	1.03	6.8	3.59	
	0.27	0.77	7.0, 16	4.01	
(4.53)	1.05	0.00	7.0, 7.3	4.87	
.290	0.00	1.35	5.8	2.77	
	0.30	0.95	5.6, 18	3.60	
(4.00)	0.61	0.64	5.7, 18	4.00	
	1.05	0.20	5.4, 18	4.18	
	1.30	0.00	7.3	4.31	PRISM $\Theta = 0^o$
.324	0.00	1.03	4.7, 6.8	1.72	
	0.27	0.77	7.1	1.93	
(4.53)	1.05	0.00	7.2	2.68	
.280	0.00	1.35	4.4, 15	1.35	
	0.30	0.95	5.8, 17	1.84	
(4.00)	0.61	0.64	5.2, 13	2.13	
	1.30	0.00	7.4	2.29	PRISM $\Theta = 60^o$
.376	0.00	0.82	5.6	1.90	
			7.1	1.69	
(4.28)			9.6	1.39	
.306	0.32	0.82	8.9	1.92	
			11.0	1.88	
(4.28)			15.0	1.63	
.306	1.14	0.00	6.8	2.28	
			7.0	2.26	
(4.28)			8.8	2.24	
			11.0	2.23	
			15.0	2.11	CYLINDER

*In attaching a model to the sidewall, the latter was replaced with an adjustable plate which altered the test section width.

Table 2 - EFFECT OF GAP WIDTH ON STROUHAL NUMBER FOR ECCENTRIC LOCATIONS OF BLUFF BODIES

Run No.	b/B Blockage	G/b Gap Width	S	Shape and Configuration
Shaw ref. (7)	0.167	0.30	.162	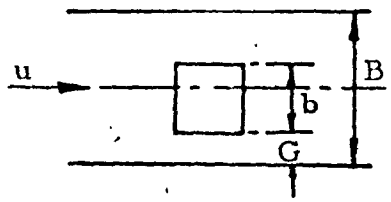
		0.63	.186	
		1.00	.189	
		1.50	.152	
		2.50	.148	
		0.00	.155	
Shaw ref. (7)	0.167	0.30	.215	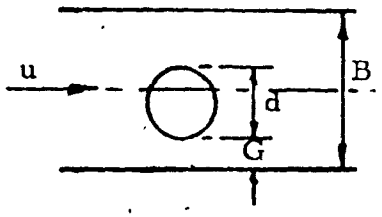
		0.63	.230	
		1.00	.232	
		1.50	.213	
		2.50	.210	
		0.00	.210	
01150260	0.061	7.735	.237	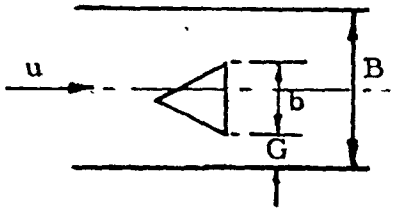
06160260		4.206	.237	
12160260		1.850	.240	
20160260		1.264	.248	
42170260		0.825	.250	
25170260		0.676	.237	
36170260		0.000	.225	
(Present)				
Shaw ref. (7)	0.056	8.429	.156	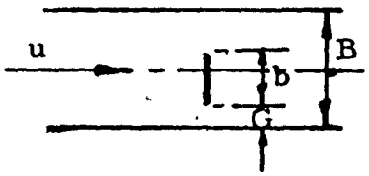
		2.529	.158	
		1.433	.161	
		0.843	.163	
		0.000	.161	
04150200	0.061	7.735	.151	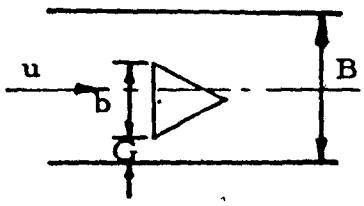
09160200		4.206	.153	
15160200		1.850	.158	
21160200		1.264	.167	
27170200		0.676	.171	
40170200		0.000	.165	
(Present)				

Table 3 - DATA OF DIRECT MEASUREMENTS

B = 14" T = 72°F

b = .85" Θ = 0°

P_{atm} = 29.7" mercury

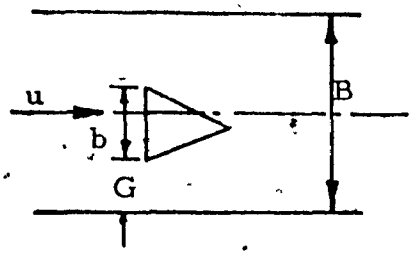

(T - Tape; Ch - Channel)

Run No.	End Gap G inch	ΔP psi	Vel. ft/sec	Filter Setting HP - cps - LP	Remarks
04150200	6.58	.36/.072	18.94	34 50	On Chart
05150200	6.58	.57/.114	23.75	40 58	On Chart
06150200	6.58	.90/.180	29.85	40 58	On Chart
09160200	3.58	.36/.072	18.94	Wide band 20/200	T. 2 Ch. 3
10160200	3.58	.55/.110	23.34	Wide band 20/200	T. 2 Ch. 4
11160200	3.58	.90/.180	29.85	40 85	On Chart
15160200	1.58	.33/.066	17.94	Wide band 20/200	T. 3 Ch. 4
16160200	1.58	.53/.106	22.80	Wide band 20/200	T. 4 Ch. 1
17160200	1.58	.90/.180	29.85	Wide band 20/200	T. 4 Ch. 2
21160200	1.07	.31/.062	17.59	Wide band 20/200	T. 5 Ch. 2
22160200	1.07	.51/.102	22.52	Wide band 20/200	T. 5 Ch. 3
23160200	1.07	.90/.180	29.85	Wide band 20/200	T. 5 Ch. 4
44170200	0.82	.90/.180	29.85	Wide band 20/200	T. 13 Ch. 3
45170200	0.82	.31/.062	17.59	Wide band 20/200	T. 13 Ch. 4
27170200	0.57	.90/.180	29.85	Wide band 20/200	T. 8 Ch. 1
28170200	0.57	.51/.102	22.52	Wide band 20/200	T. 8 Ch. 2
29170200	0.57	.31/.062	17.59	Wide band 20/200	T. 8 Ch. 3
39170200	0.00	.90/.180	29.85	Wide band 20/200	T. 12 Ch. 1
40170200	0.00	.56/.112	23.59	Wide band 20/200	T. 12 Ch. 2
41170200	0.00	.36/.072	18.94	Wide band 20/200	T. 12 Ch. 3

Table 4 - DATA OF DIRECT MEASUREMENTS

B = 14" T = 72°F

b = .85" Θ = 60°

P_{atm} = 29.7" mercury

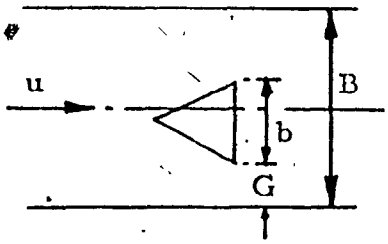

(T - Tape; Ch - Channel)

Run No.	End Gap G inch	ΔP psi	Vel. ft/sec	Filter Setting HP - cps - LP	Remarks
01150260	6.58	.90/.180	29.85	94 112	On Chart
02150260	6.58	.57/.114	23.75	65 100	On Chart
03150260	6.58	.36/.072	18.94	54 78	On Chart
06160260	3.58	.90/.180	29.85	95 120	On Chart
07160260	3.58	.55/.110	23.34	Wide band 20/200	T. 2 Ch. 1
08160260	3.58	.36/.072	18.94	Wide band 20/200	T. 2 Ch. 2
12160260	1.58	.90/.180	29.85	Wide band 20/200	T. 3 Ch. 1
13160260	1.58	.55/.110	23.34	Wide band 20/200	T. 3 Ch. 2
14160260	1.58	.36/.072	18.94	Wide band 20/200	T. 3 Ch. 3
18160260	1.07	.90/.180	29.85	Wide band 20/200	T. 4 Ch. 3
19160260	1.07	.53/.106	22.80	Wide band 20/200	T. 4 Ch. 4
20160260	1.07	.33/.066	17.94	Wide band 20/200	T. 5 Ch. 1
42170260	0.82	.31/.062	17.59	Wide band 20/200	T. 13 Ch. 1
43170260	0.82	.89/.178	29.85	Wide band 20/200	T. 13 Ch. 2
24170260	0.57	.32/.064	17.75	Wide band 20/200	T. 7 Ch. 1
25170260	0.57	.51/.102	22.52	Wide band 20/200	T. 7 Ch. 2
26170260	0.57	.90/.180	29.85	Wide band 20/200	T. 7 Ch. 3
36170260	0.00	.36/.072	18.94	Wide band 20/200	T. 11 Ch. 1
37170260	0.00	.56/.112	23.59	Wide band 20/200	T. 11 Ch. 2
38170260	0.00	.90/.180	29.85	Wide band 20/200	T. 11 Ch. 3

Table 5

B = 14" T = 72°F

b = .85" Θ = 0°

P_{atm} = 29.7" mercury

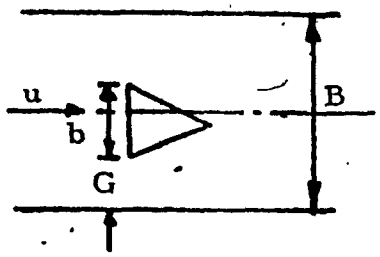

Run No.	End Gap, G inch	Velocity ft/sec	Frequency f	$R \times 10^5$	S
04150200	6.58	18.94	40.0	2.46	0.151
05150200	6.58	23.75	50.0	3.09	0.149
06150200	6.58	29.85	62.0	3.88	0.149
09160200	3.58	18.94	41.0	2.46	0.153
10160200	3.58	23.34	50.0	3.03	0.152
11160200	3.58	29.85	64.0	3.88	0.152
15160200	1.58	17.94	40.0	2.33	0.167
16160200	1.58	22.80	51.0	2.96	0.167
17160200	1.58	29.85	67.0	3.88	0.166
27170200	0.57	29.85	72.0	3.88	0.171
28170200	0.57	22.52	54.0	2.93	0.170
39170200	0.00	29.85	70.0	3.88	0.166
40170200	0.00	23.59	55.0	3.07	0.165

Table 6

B = 14" T = 72°F

b = .85" Θ = 60°

P_{atm} = 29.7" mercury

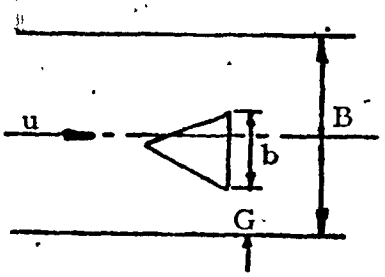

Run No.	End Gap G inch	Velocity ft/sec	Frequency f	R x 10^5	S
01150260	6.58	29.85	100.0	3.88	0.237
02150260	6.58	23.75	80.0	3.09	0.239
03150260	6.58	18.94	63.0	2.46	0.238
06160260	3.58	29.85	100.0	3.88	0.237
07160260	3.58	23.34	79.0	3.03	0.240
08160260	3.58	18.94	63.0	2.46	0.236
12160260	1.58	29.85	101.0	3.88	0.240
13160260	1.58	23.34	79.5	3.03	0.241
14160260	1.58	18.94	64.0	2.46	0.240
18160260	1.07	29.85	103.0	3.88	0.244
19160260	1.07	22.80	80.0	2.96	0.249
20160260	1.07	17.94	63.0	2.33	0.248
42170260	0.82	17.59	62.0	2.29	0.250
43170260	0.82	29.85	103.0	3.88	0.249
36170260	0.00	18.94	60.0	2.46	0.225
37170260	0.00	23.59	75.0	3.07	0.225
38170260	0.00	29.85	95.0	3.88	0.225

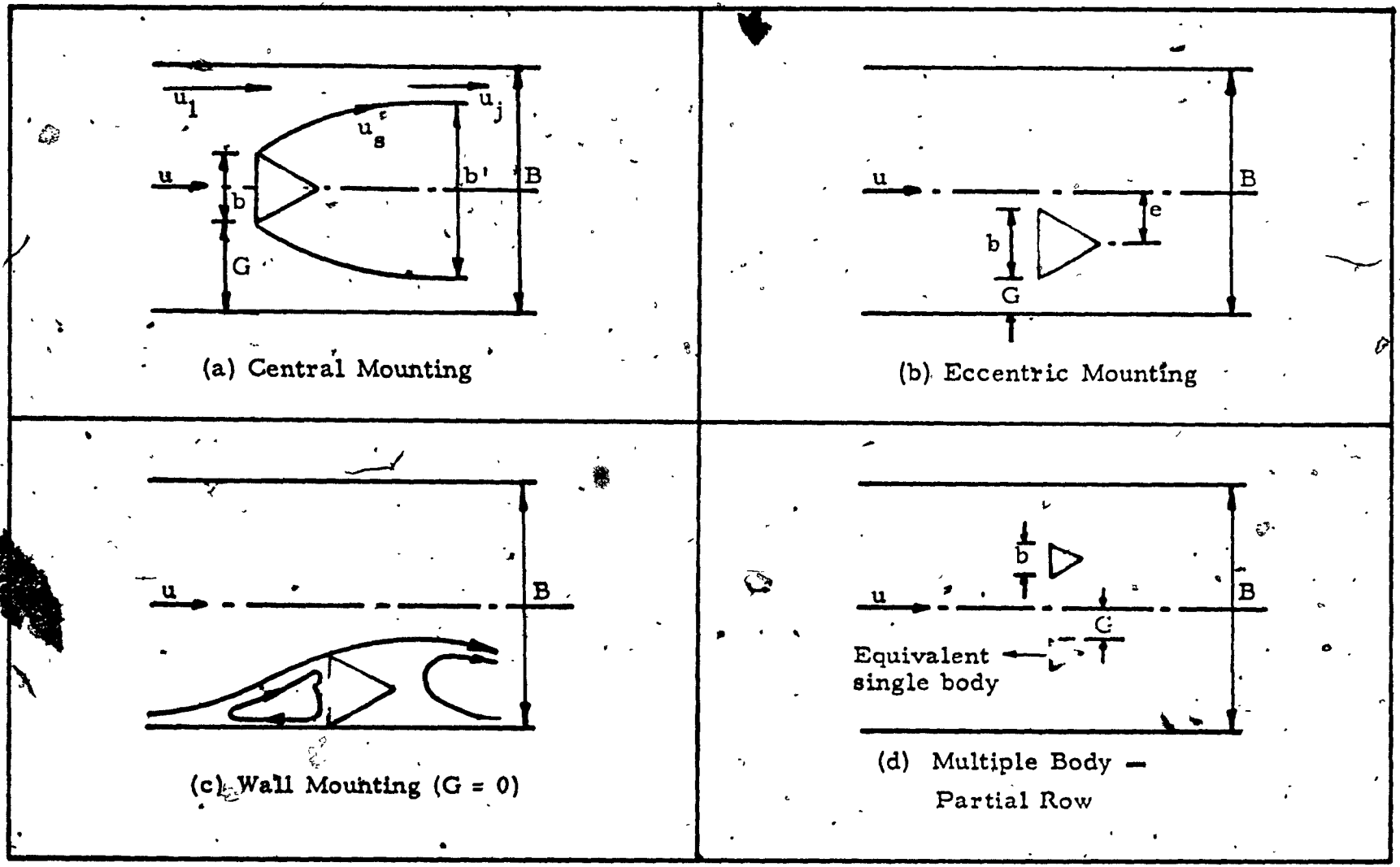

FLOW PAST A PRISM ($\theta = 0^\circ$)

Fig. 1

PRISMS

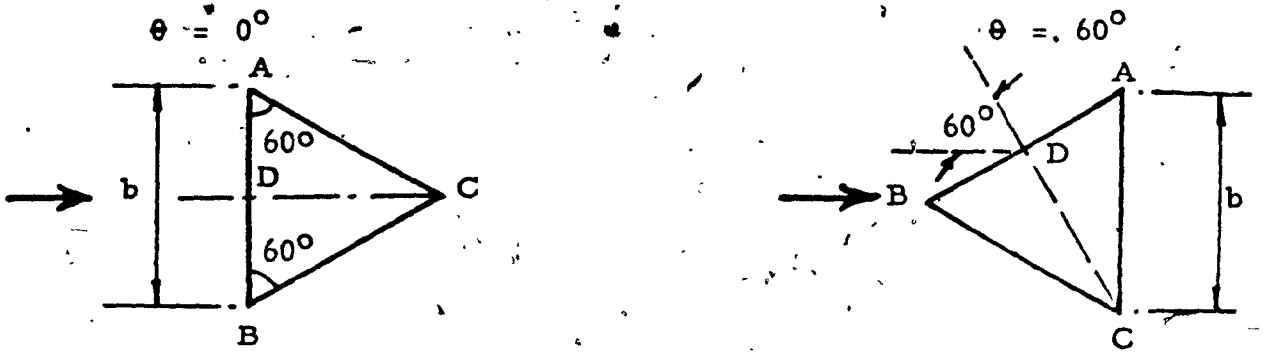

b	b/B	G/b
0.85	0.061	0.0 - 7.735

TEST BODIES

Fig. 2

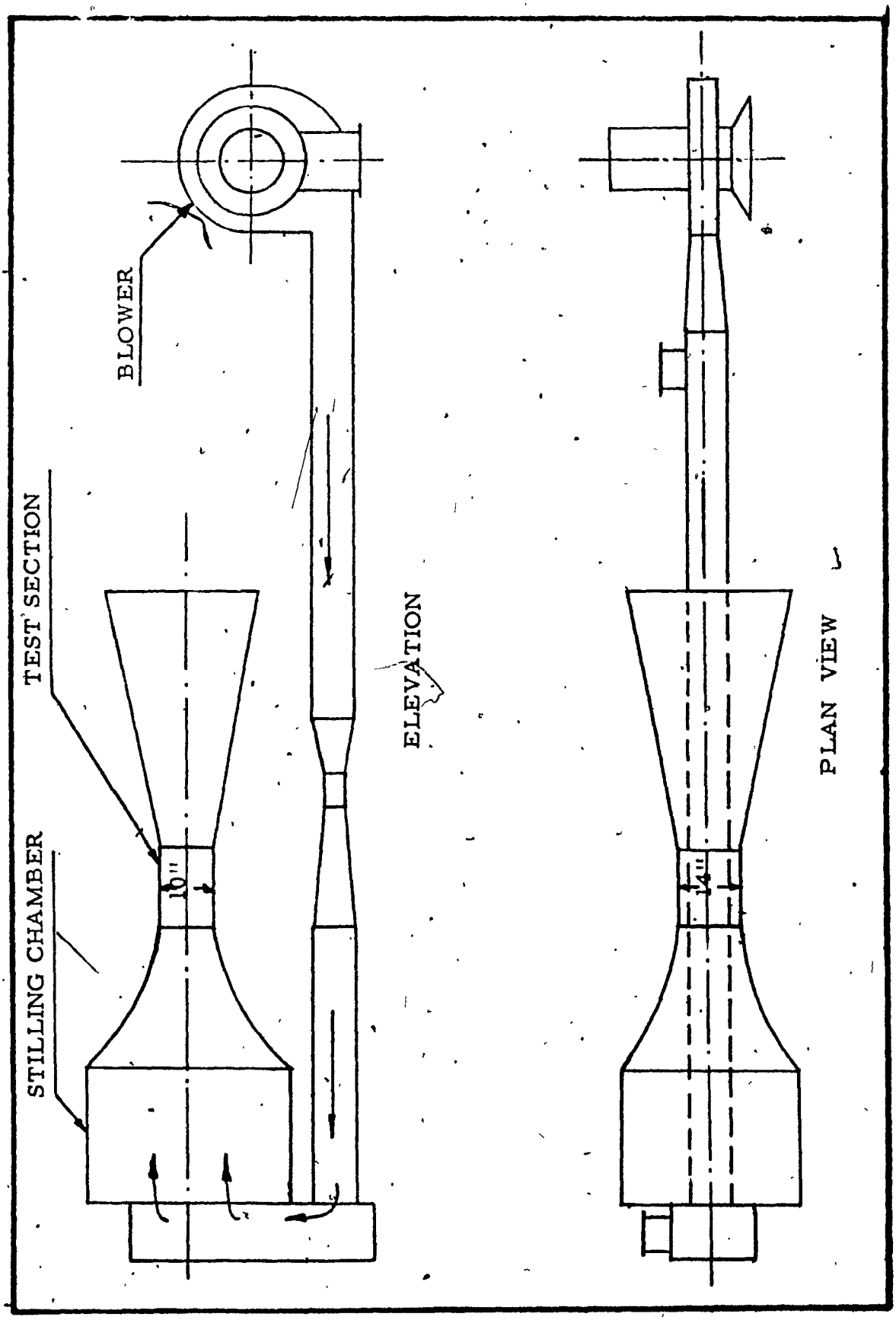

WIND TUNNEL

Fig. 3

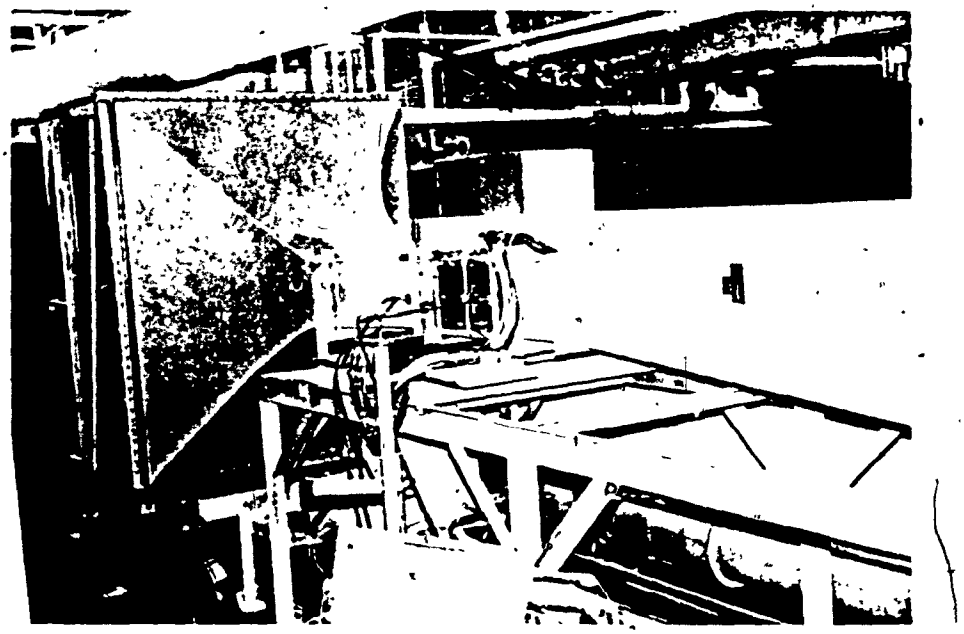

WIND TUNNEL SIDE VIEW

Fig. 4(a)

WIND TUNNEL END VIEW

Fig. 4(b)

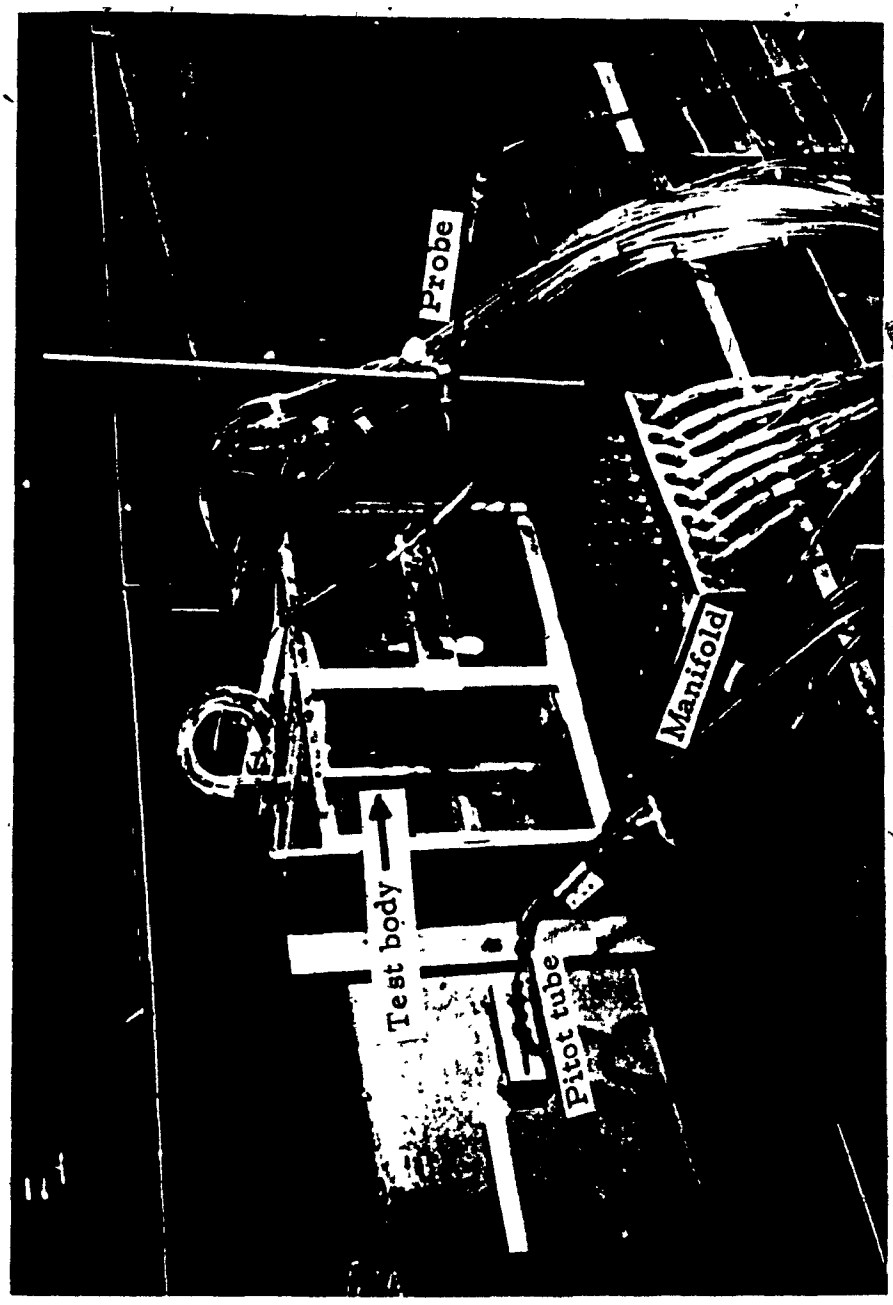

WIND TUNNEL TEST SECTION

Fig. 5

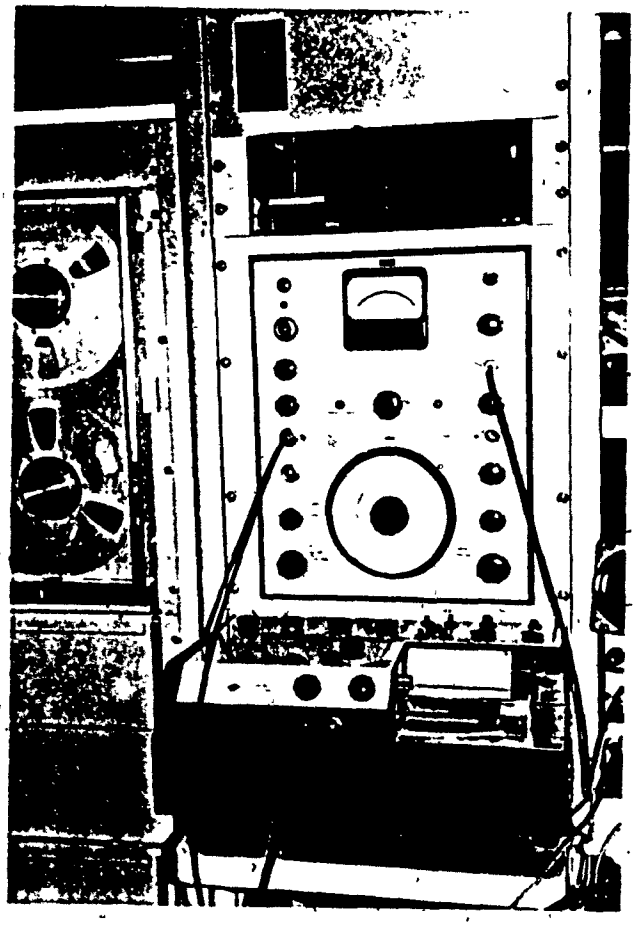

WAVE ANALYZER

Fig. 6

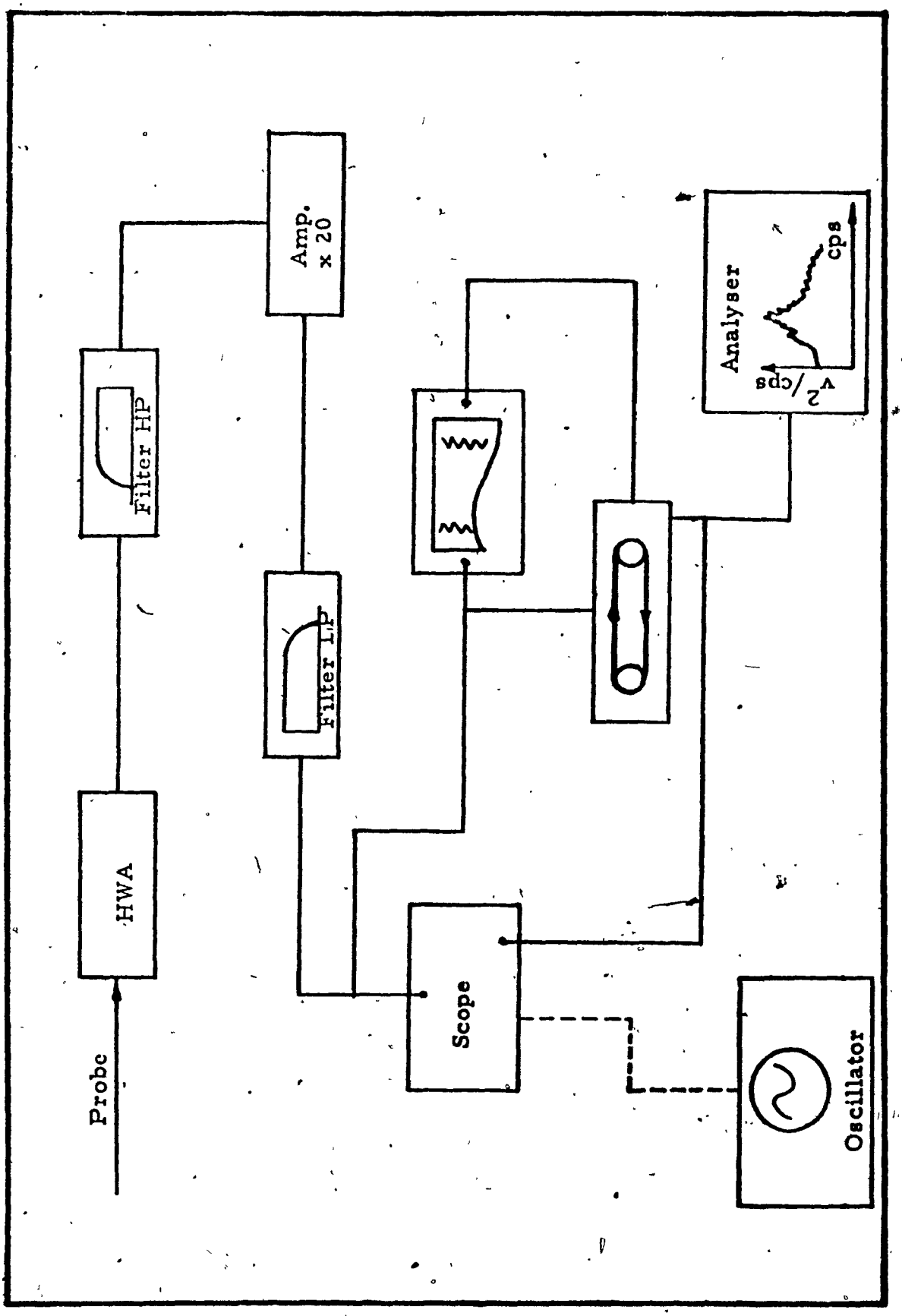

DATA ACQUISITION SYSTEM

Fig. 7

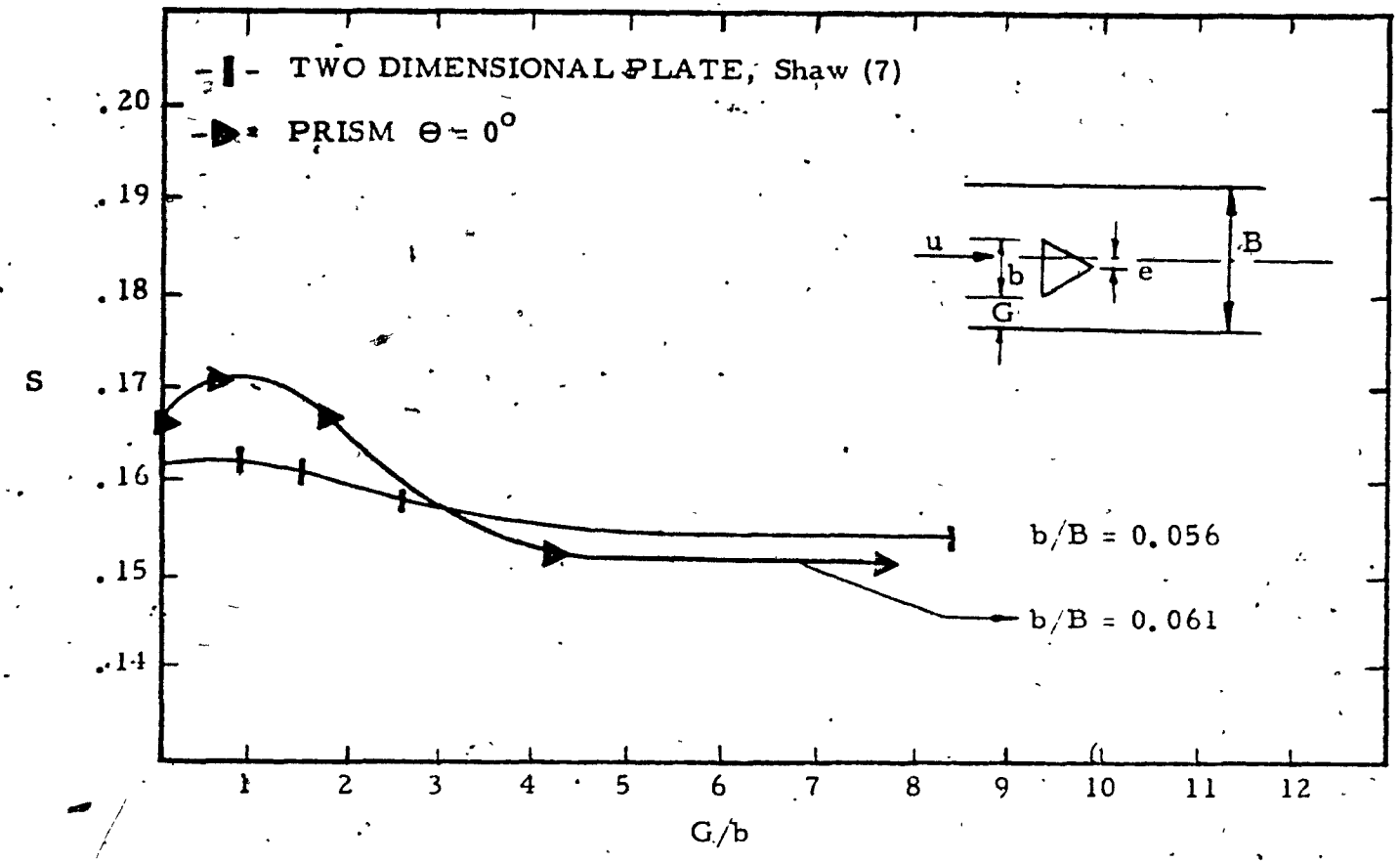

EFFECT OF GAP WIDTH ON STROUHAL NUMBER FOR ECCENTRIC LOCATIONS OF BLUFF BODIES (Ref. 7)

Fig. 8

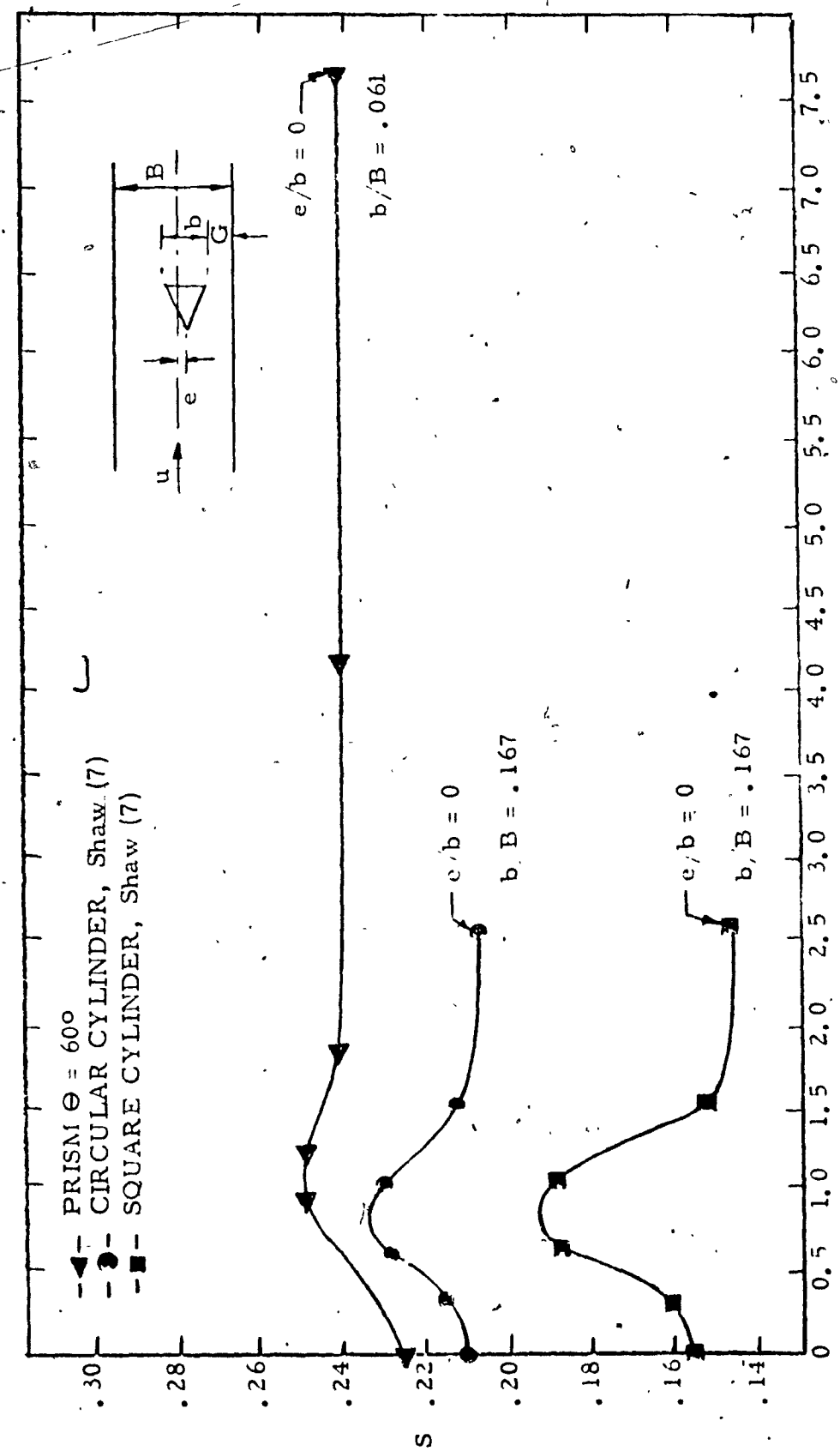

EFFECT OF GAP WIDTH ON STROUHAL NUMBER FOR ECCENTRIC LOCATIONS OF BLUFF BODIES (Ref: 7)

Fig. 9

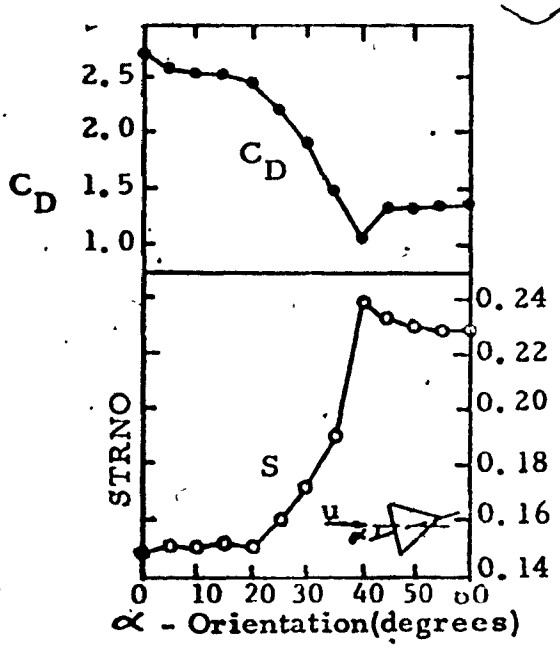

Coefficients of Mean Drag, C_D, and the Strouhal Number, STRNO, for an Equilateral Triangular Cylinder as Function of Attitude Angle α. (Ref. 11)

Mean Drag Coefficient and Inverse of Strouhal Number vs. Reynolds Number. (S = Strouhal Number)

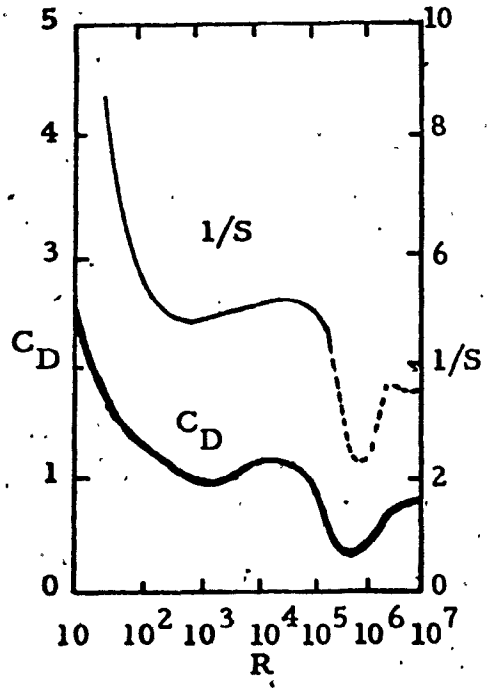

VARIATION OF DRAG COEFFICIENT AND STROUHAL NUMBER FOR BLUFF BODIES

Fig. 10

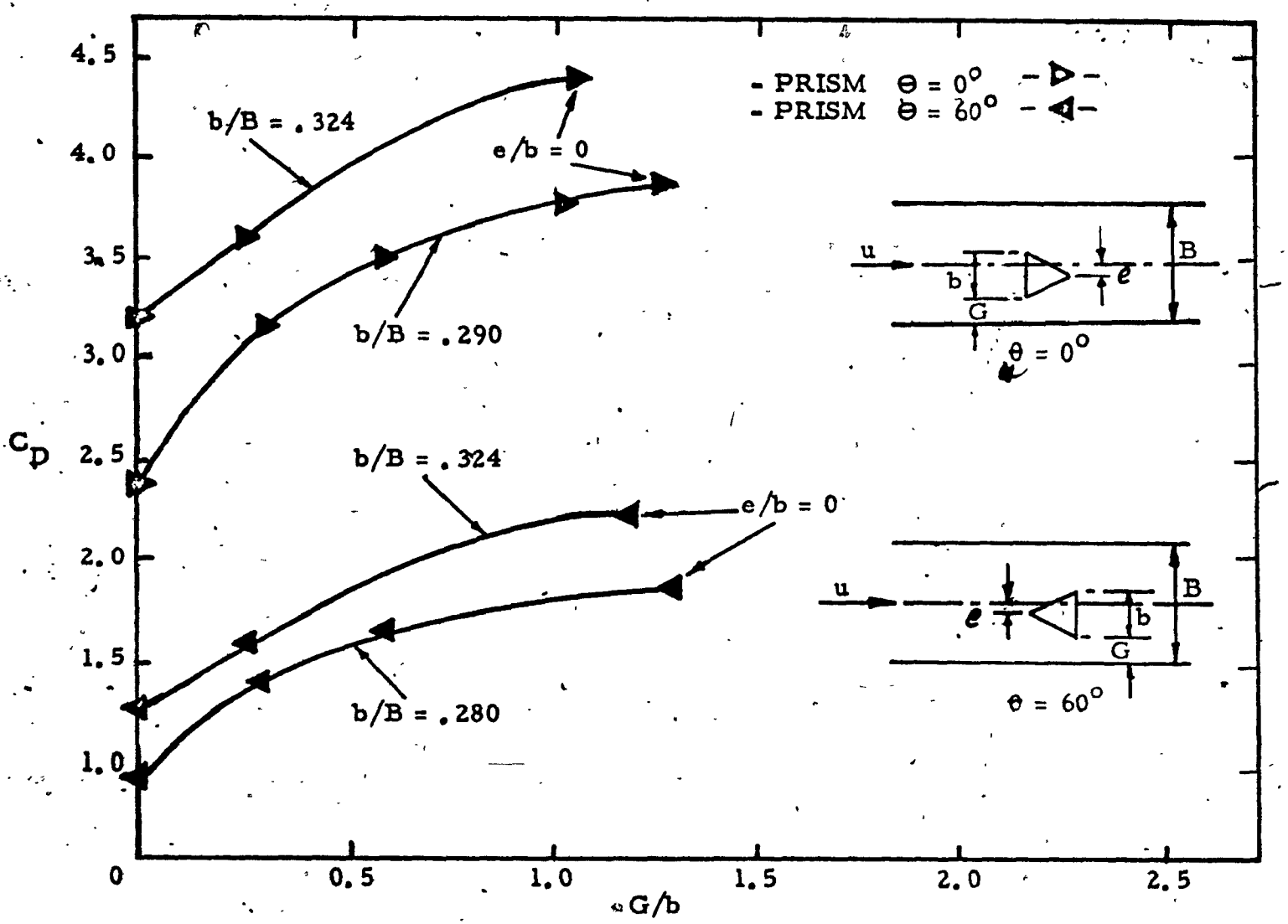

DRAG COEFFICIENTS FOR ECCENTRIC LOCATIONS (Ref. 8 and 9)

Fig. 11

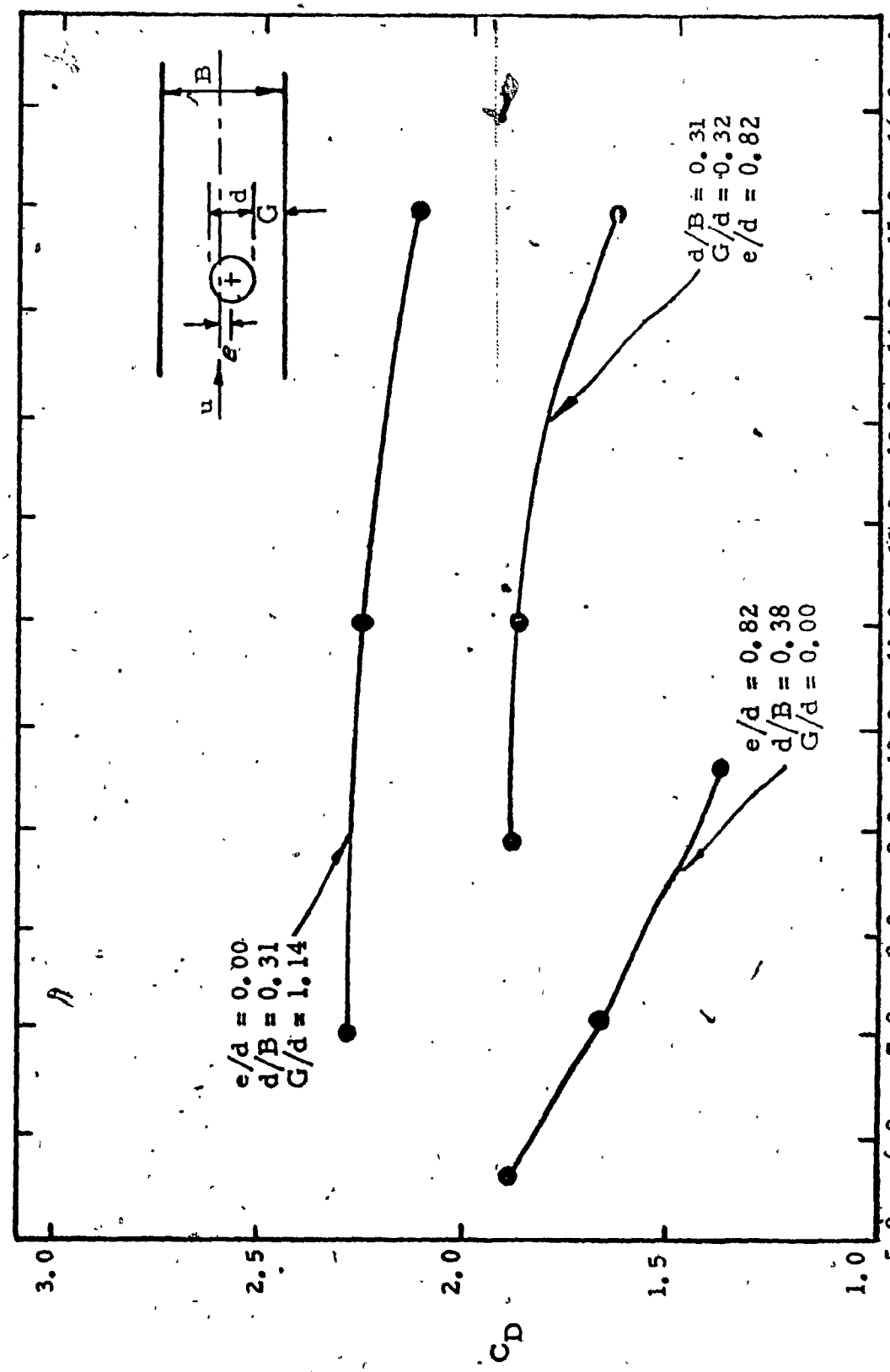

DRAG COEFFICIENTS FOR ECCENTRIC LOCATIONS (Ref. 8 and 9)

Fig. 12

Fig. 13 - STRIP CHART RECORDS (See Table 3)
EFFECT OF GAP ON VORTEX SHEDDING

b/B = 0.061
Θ = 0^{o}
V = 29.85 ft/sec
Chart speed: 125 mm/sec

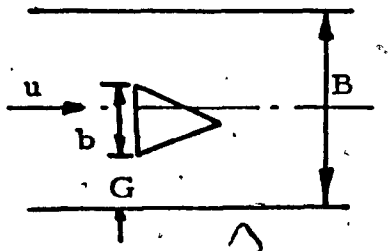

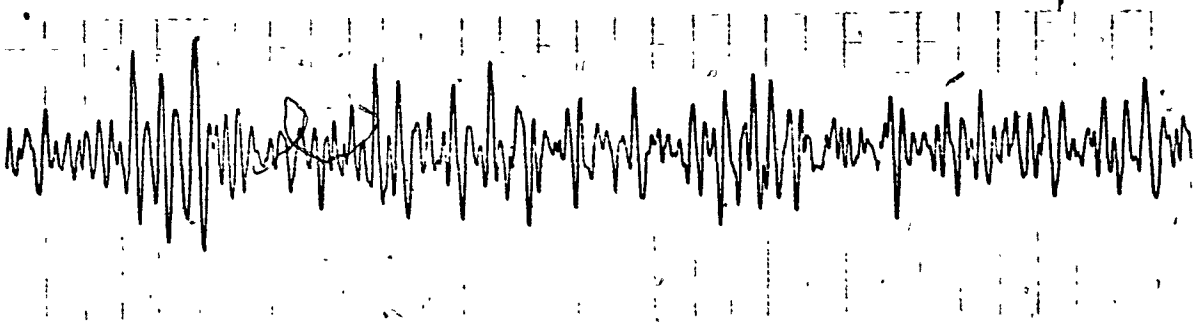

Run No. 06150200 G = 6.58

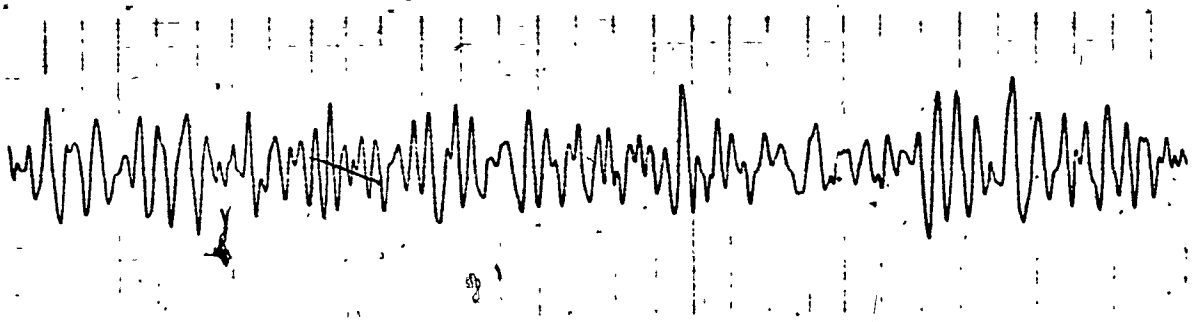

Run No. 11160200 G = 3.58

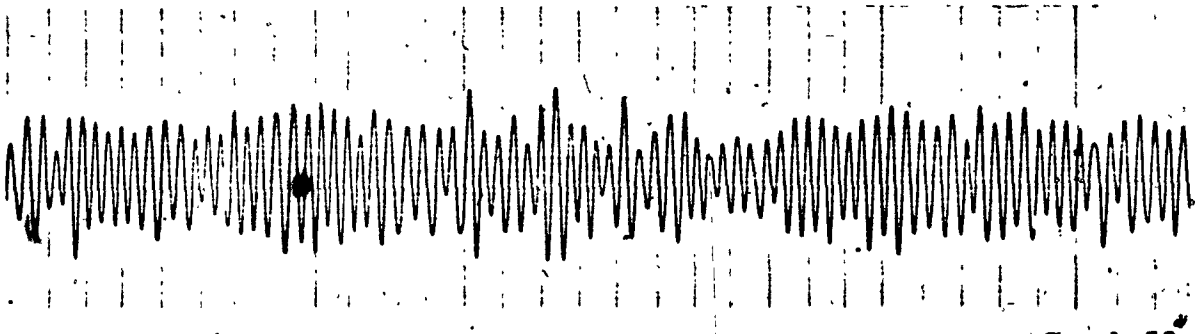

Run No. 17160200 G = 1.58

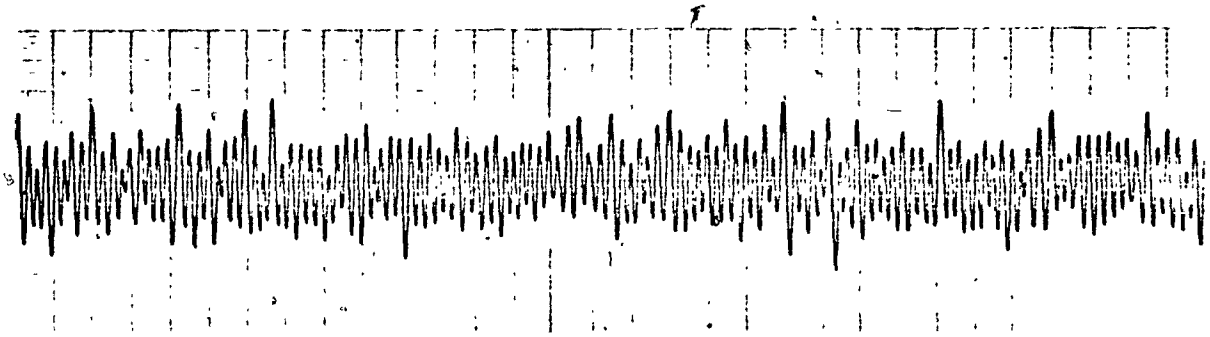

Run No. 18160260 G = 1.07"

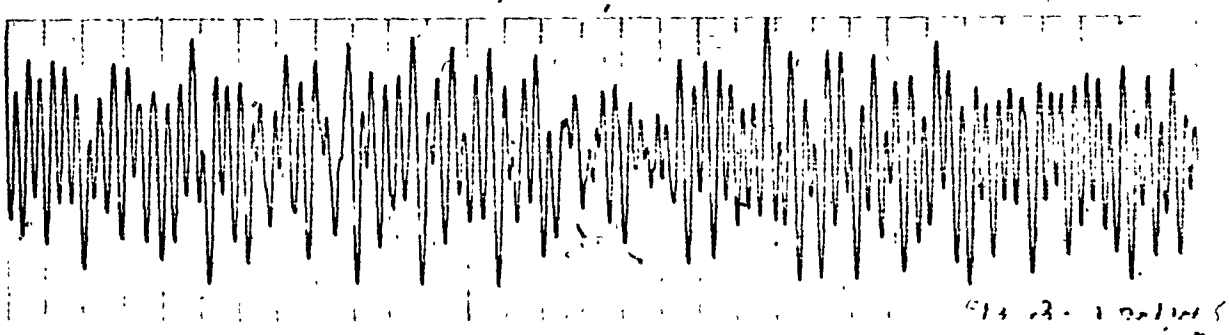

Run No. 43170260 G = 0.82"

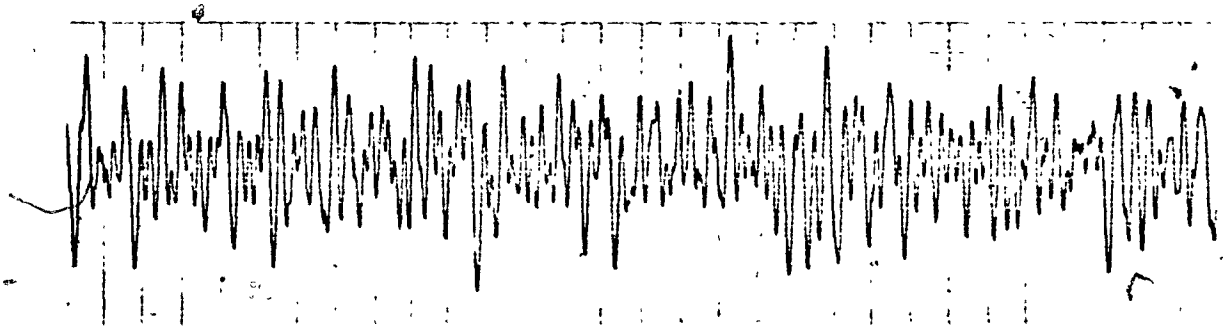

Run No. 26170260 G = 0.57"

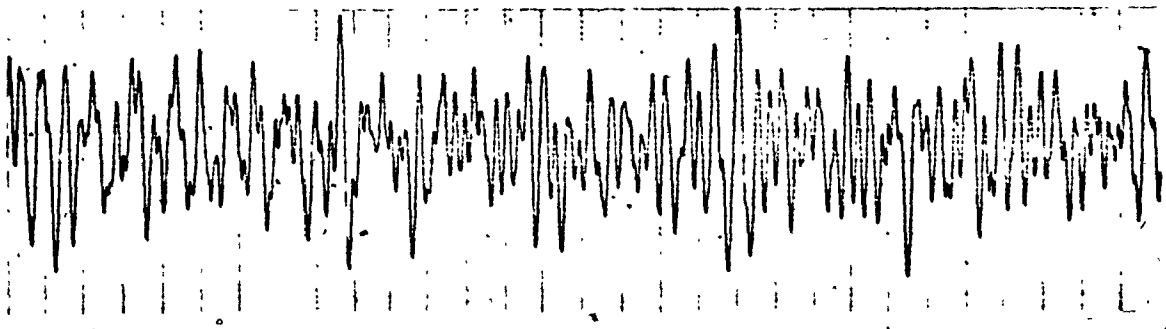

Run No. 38170260 G = 0.00"

Fig. 14 - STRIP CHART RECORDS (See Table 4)
EFFECT OF GAP ON VORTEX SHEDDING

b/B = 0.061
Θ = 60°
V = 29.85 ft/sec
Chart speed: 125 mm/sec

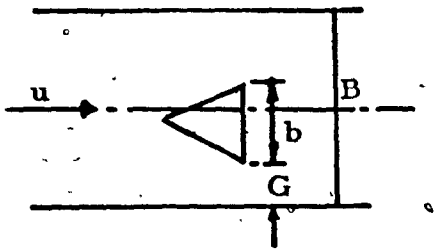

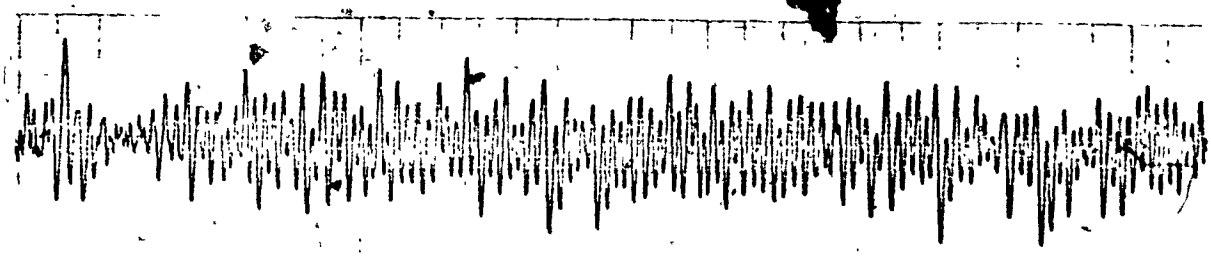

Run No. 01150260 G = 6.58

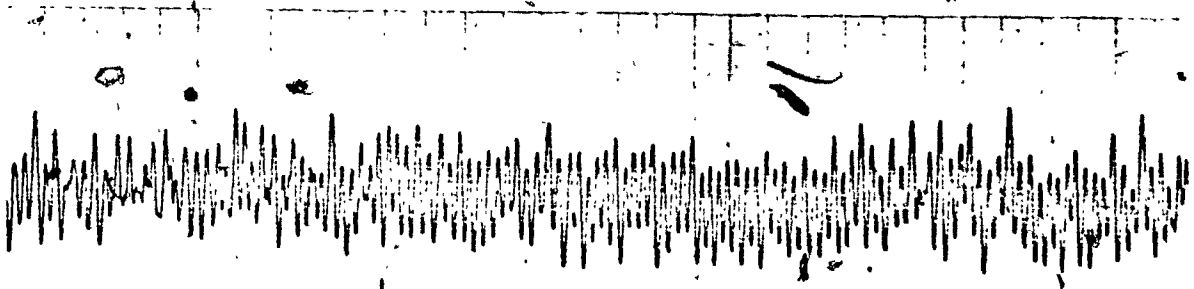

Run No. 06160260 G = 3.58

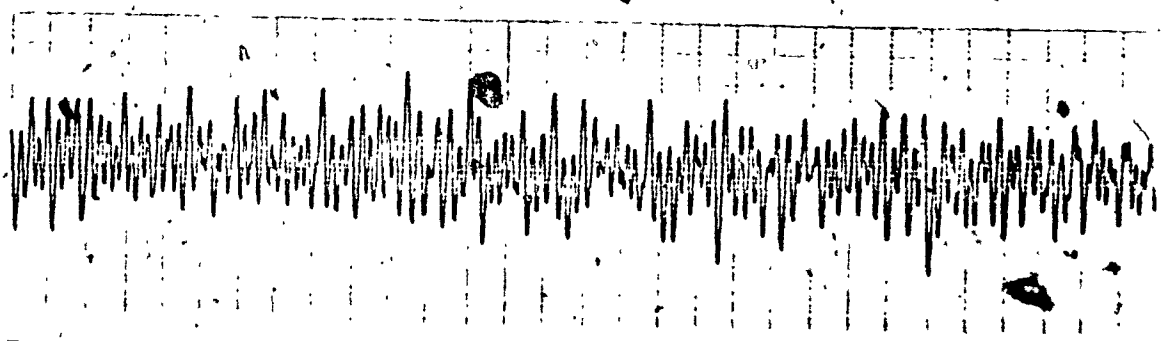

Run No. 12160260 G = 1.58

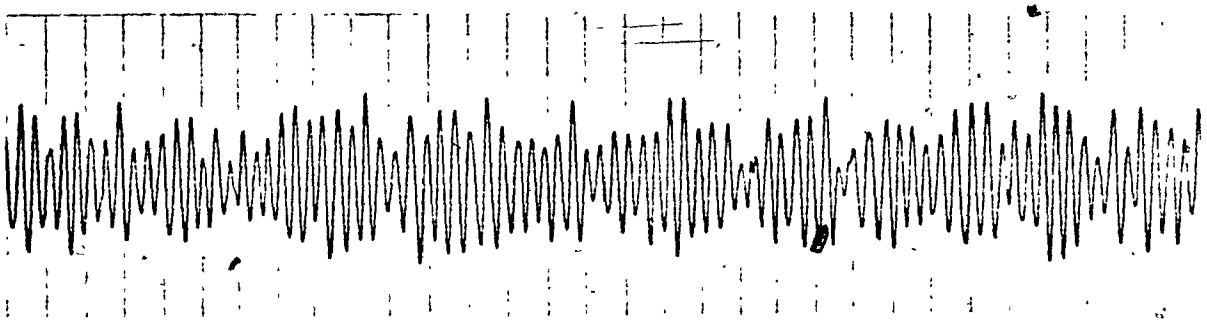

Run No. 23160200 G = 1.07"

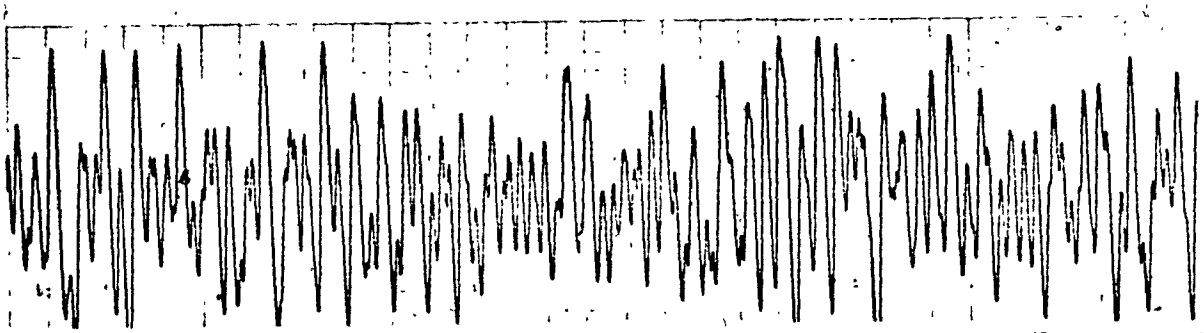

Run No. 44170200 G = 0.82"

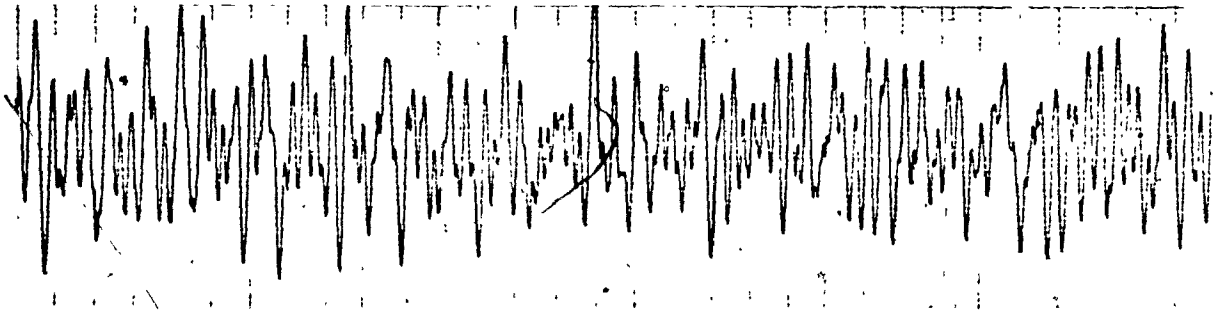

Run No. 27170200 G = 0.57"

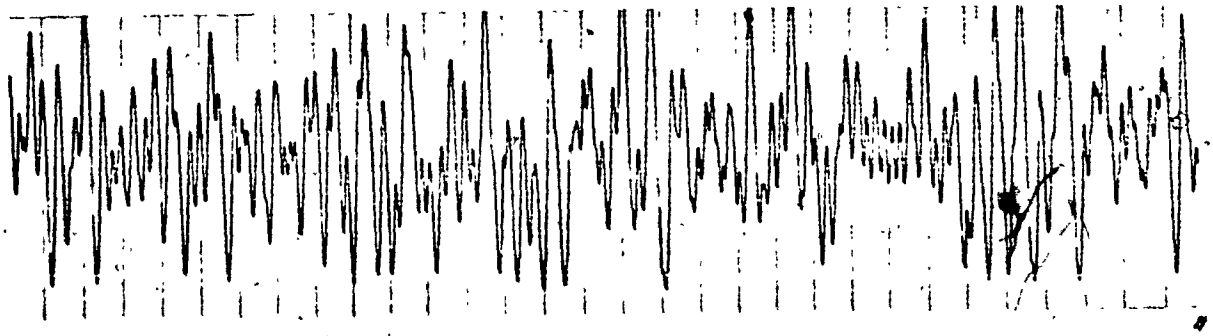

Run No. 39170200 G = 0.00"

Fig. 15 - POWER DENSITY SPECTRA - VORTEX SHEDDING
(See Table 5)

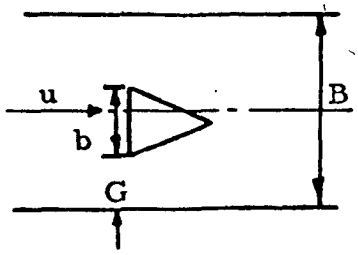

b/B = 0.061
Θ = 0°
Record speed: 1.875 ips
Playback speed: 1.875 ips

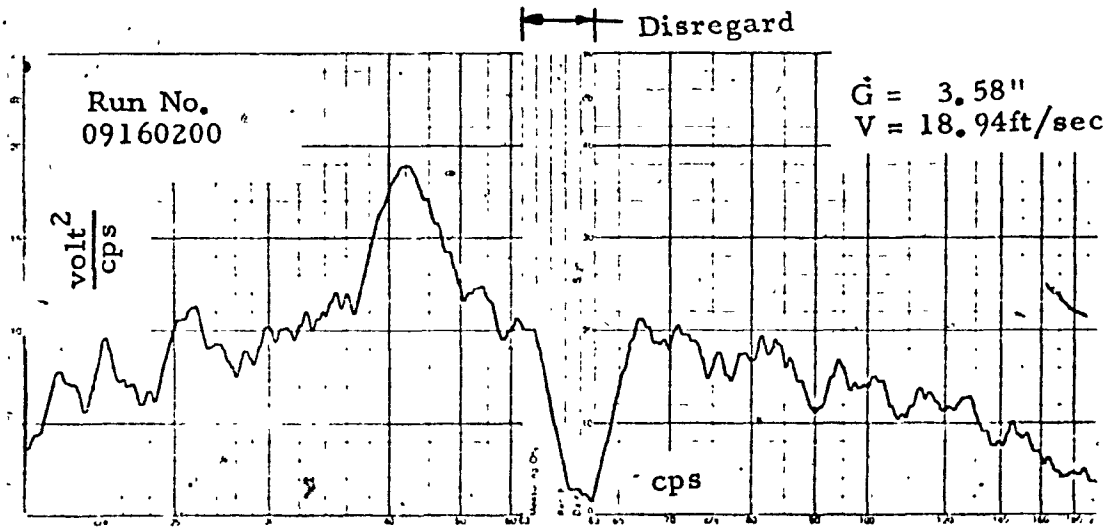

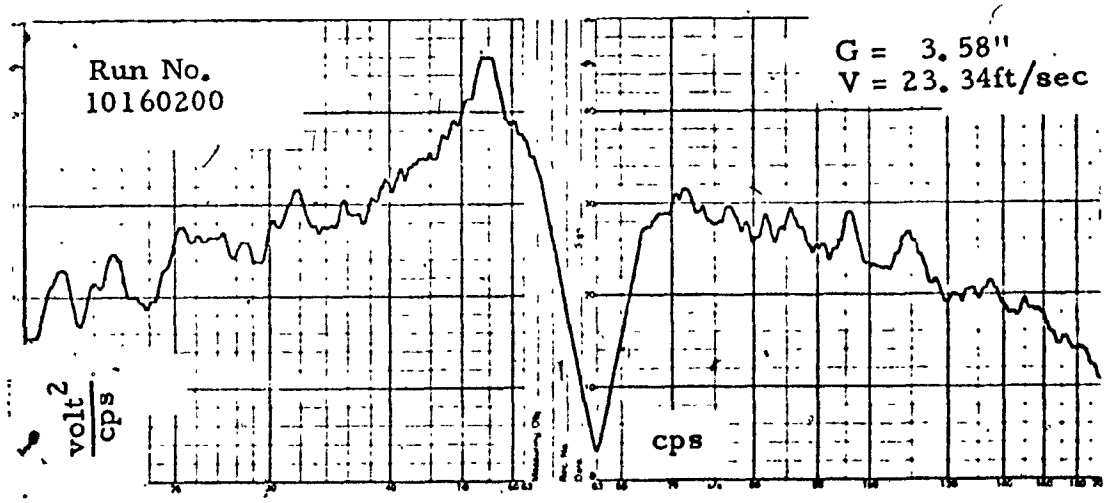

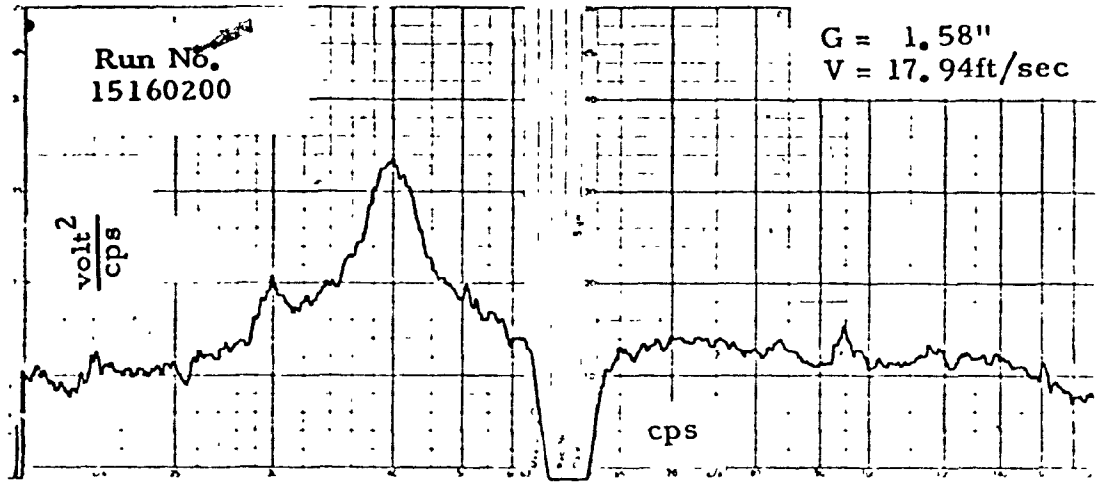
Run No.
15160200
G = 1.58"
V = 17.94ft/sec
volt²/cps
cps

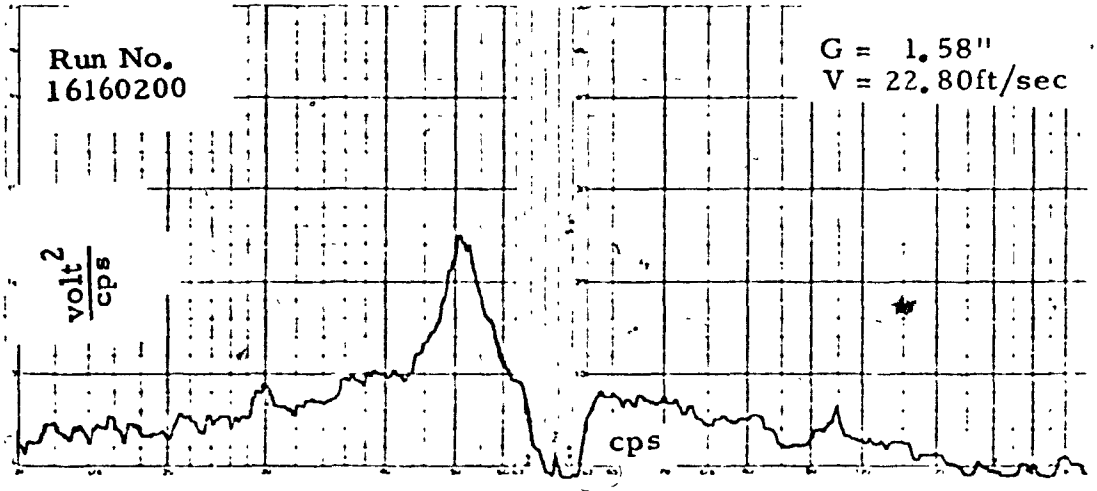
Run No.
16160200
G = 1.58"
V = 22.80ft/sec
volt²/cps
cps

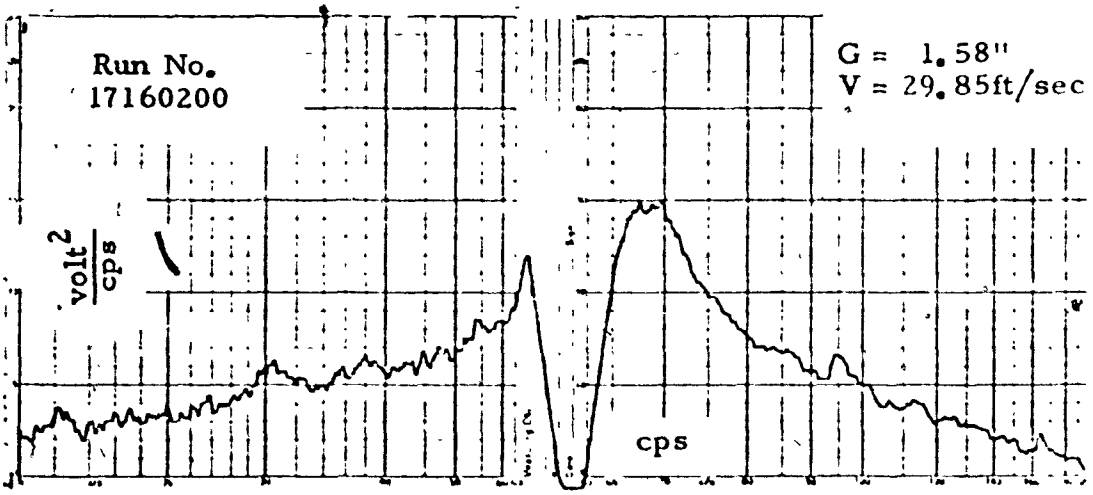
Run No.
17160200
G = 1.58"
V = 29.85ft/sec
volt²/cps
cps

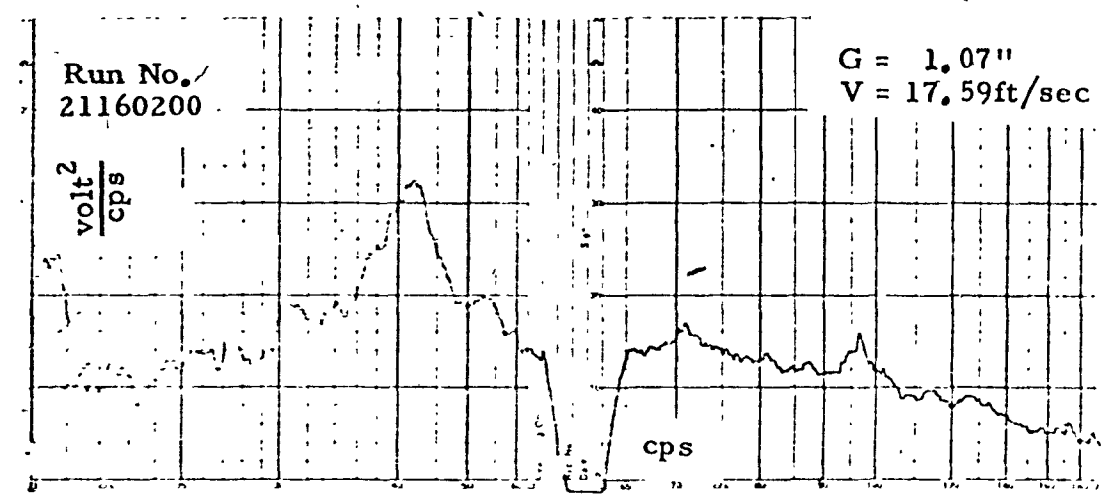
Run No.
21160200
G = 1.07"
V = 17.59ft/sec
volt²/cps
cps

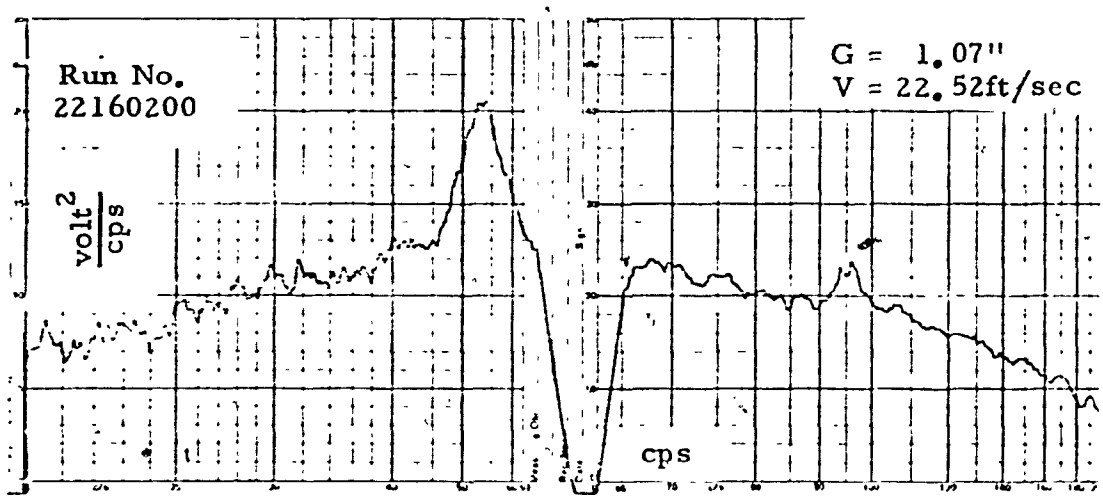
Run No.
22160200
G = 1.07"
V = 22.52ft/sec
volt²/cps
cps

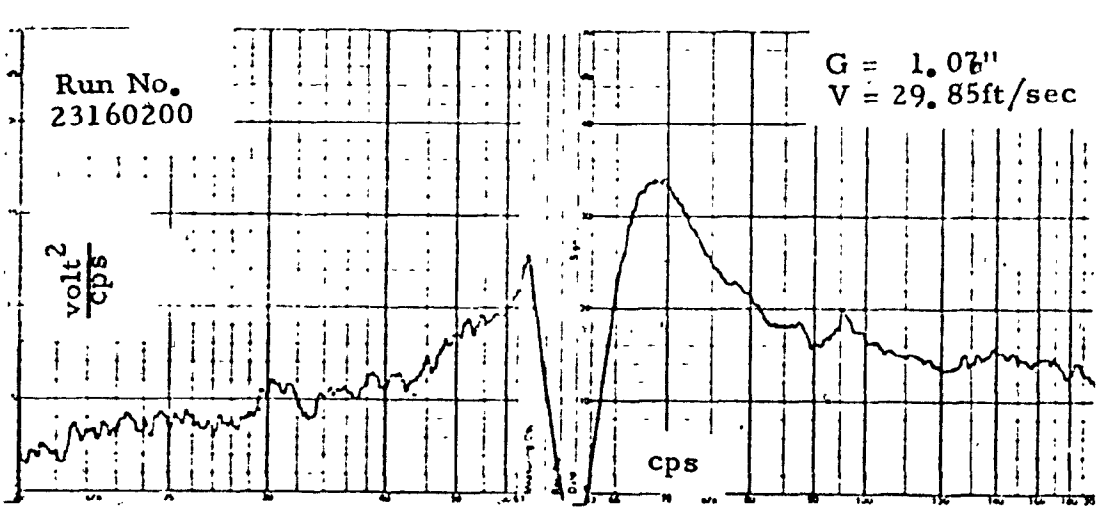
Run No.
23160200
G = 1.07"
V = 29.85ft/sec
volt²/cps
cps

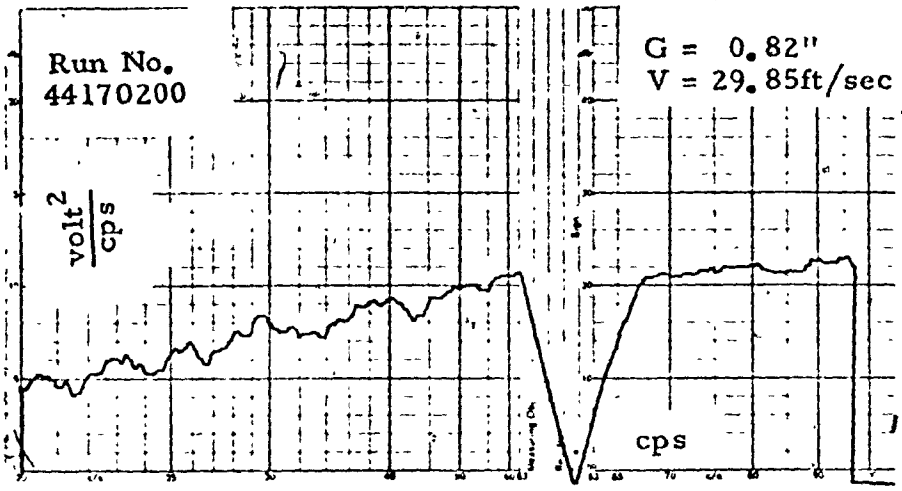
Run No.
44170200
G = 0.82"
V = 29.85ft/sec
volt²/cps
cps

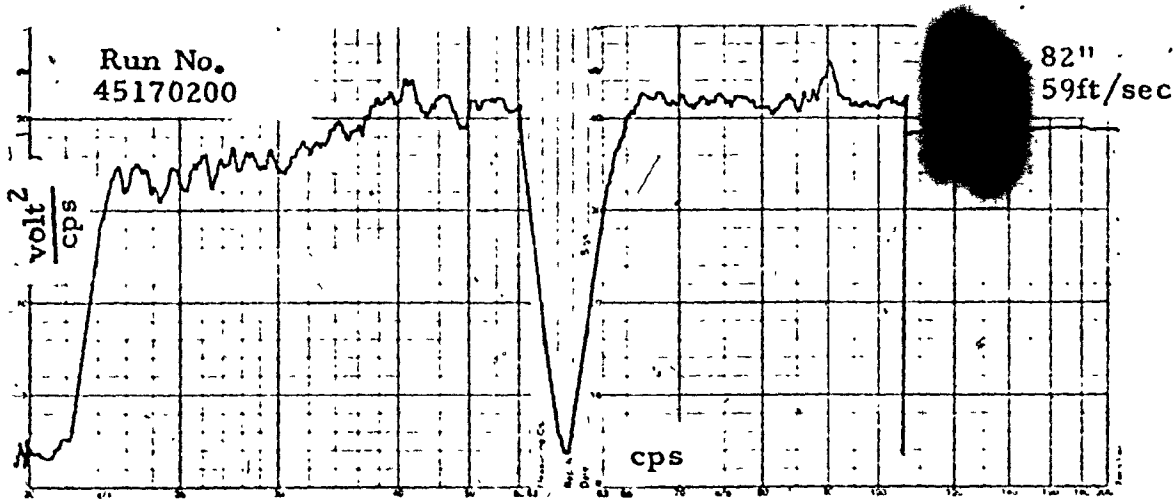
Run No.
45170200
82"
59ft/sec
volt²/cps
cps

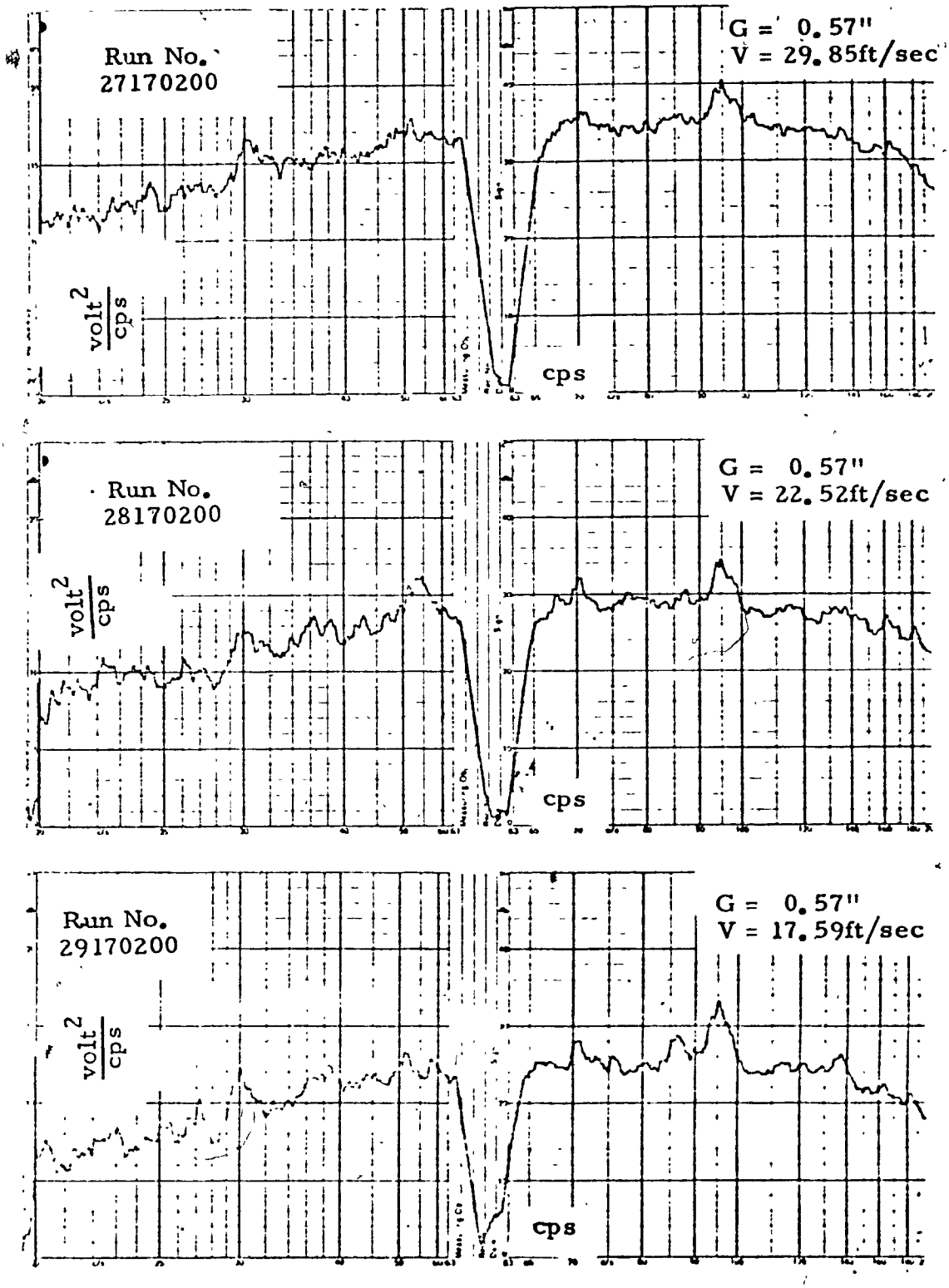
Run No.
27170200
G = 0.57"
V = 29.85ft/sec
volt²/cps
cps
Run No.
28170200
G = 0.57"
V = 22.52ft/sec
volt²/cps
cps
Run No.
29170200
G = 0.57"
V = 17.59ft/sec
volt²/cps
cps

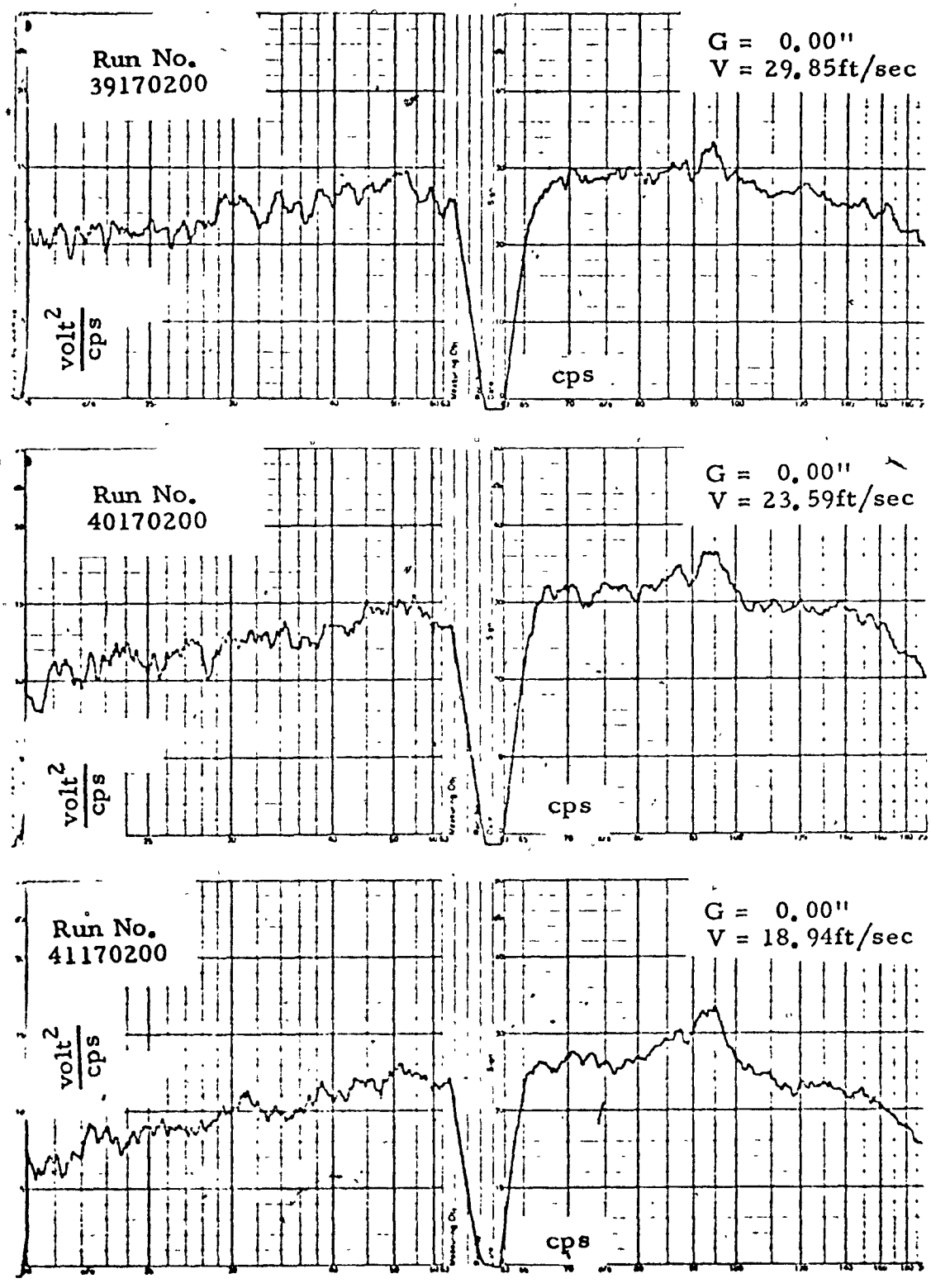
Run No.
39170200
G = 0.00"
V = 29.85ft/sec
volt² / cps
cps
Run No.
40170200
G = 0.00"
V = 23.59ft/sec
volt² / cps
cps
Run No.
41170200
G = 0.00"
V = 18.94ft/sec
volt² / cps
cps

Fig. 16 - POWER DENSITY SPECTRA - VORTEX SHEDDING
(See Table 6)

b/B = 0.061
Θ = 60°
Record speed: 1.875 ips
Playback speed: 1.875 ips

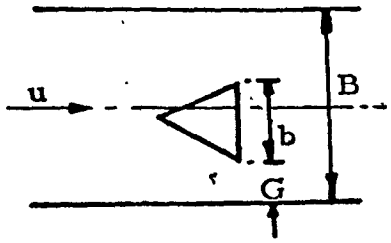

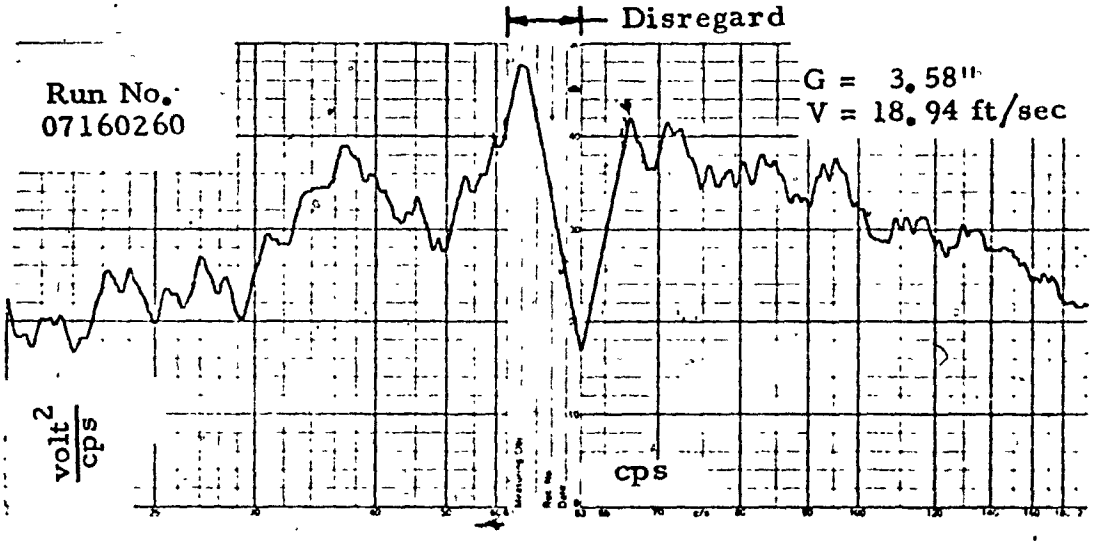

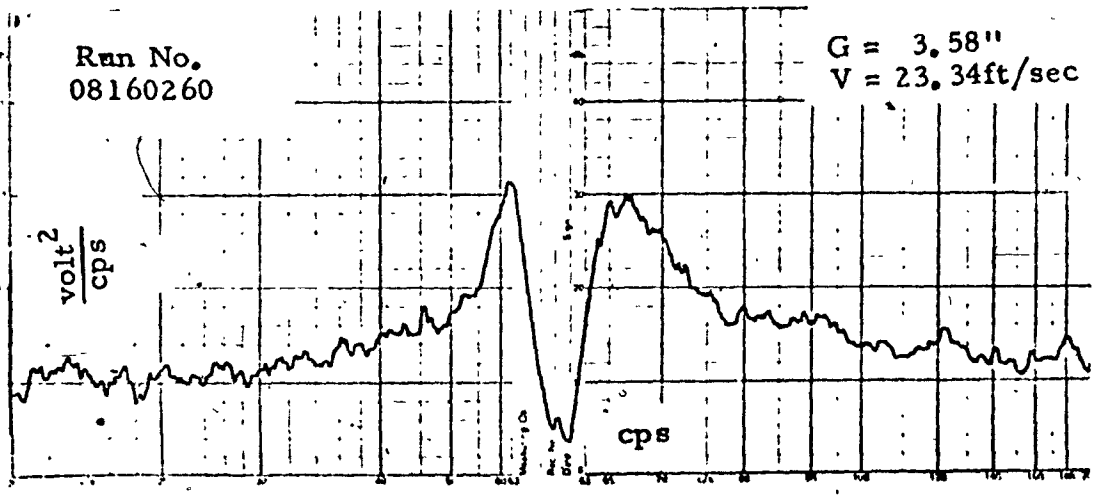

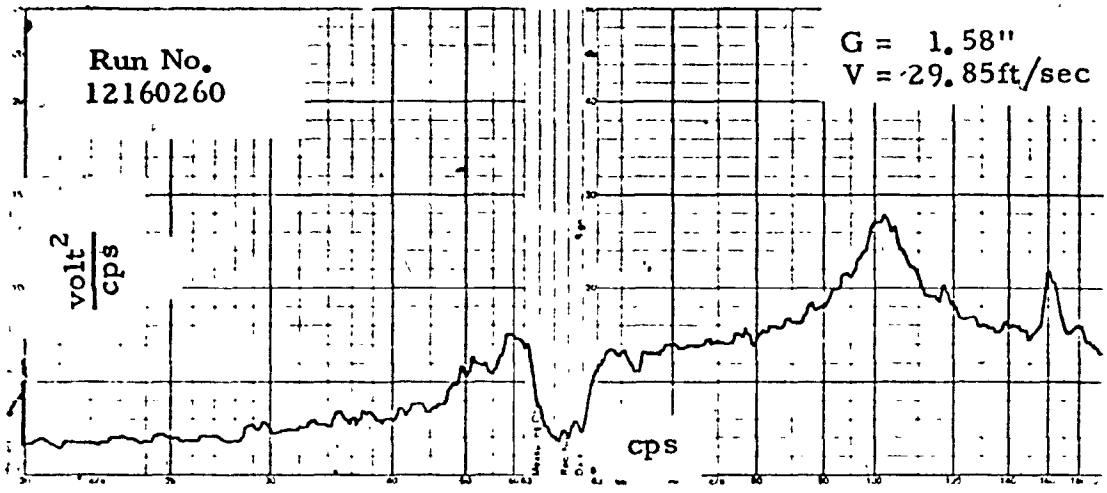
Run No.
12160260
G = 1.58"
V = 29.85ft/sec
volt²/cps
cps

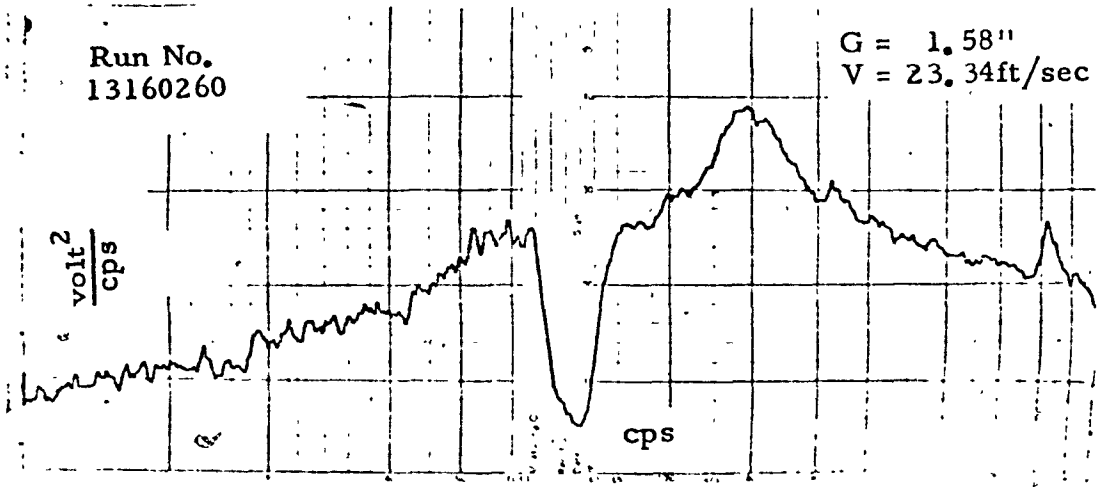
Run No.
13160260
G = 1.58"
V = 23.34ft/sec
volt²/cps
cps

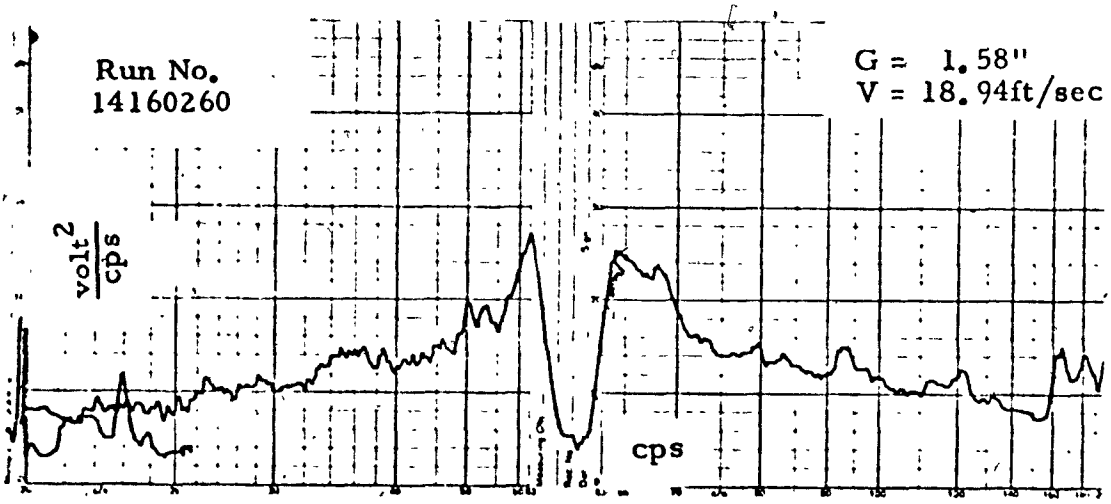
Run No.
14160260
G = 1.58"
V = 18.94ft/sec
volt²/cps
cps

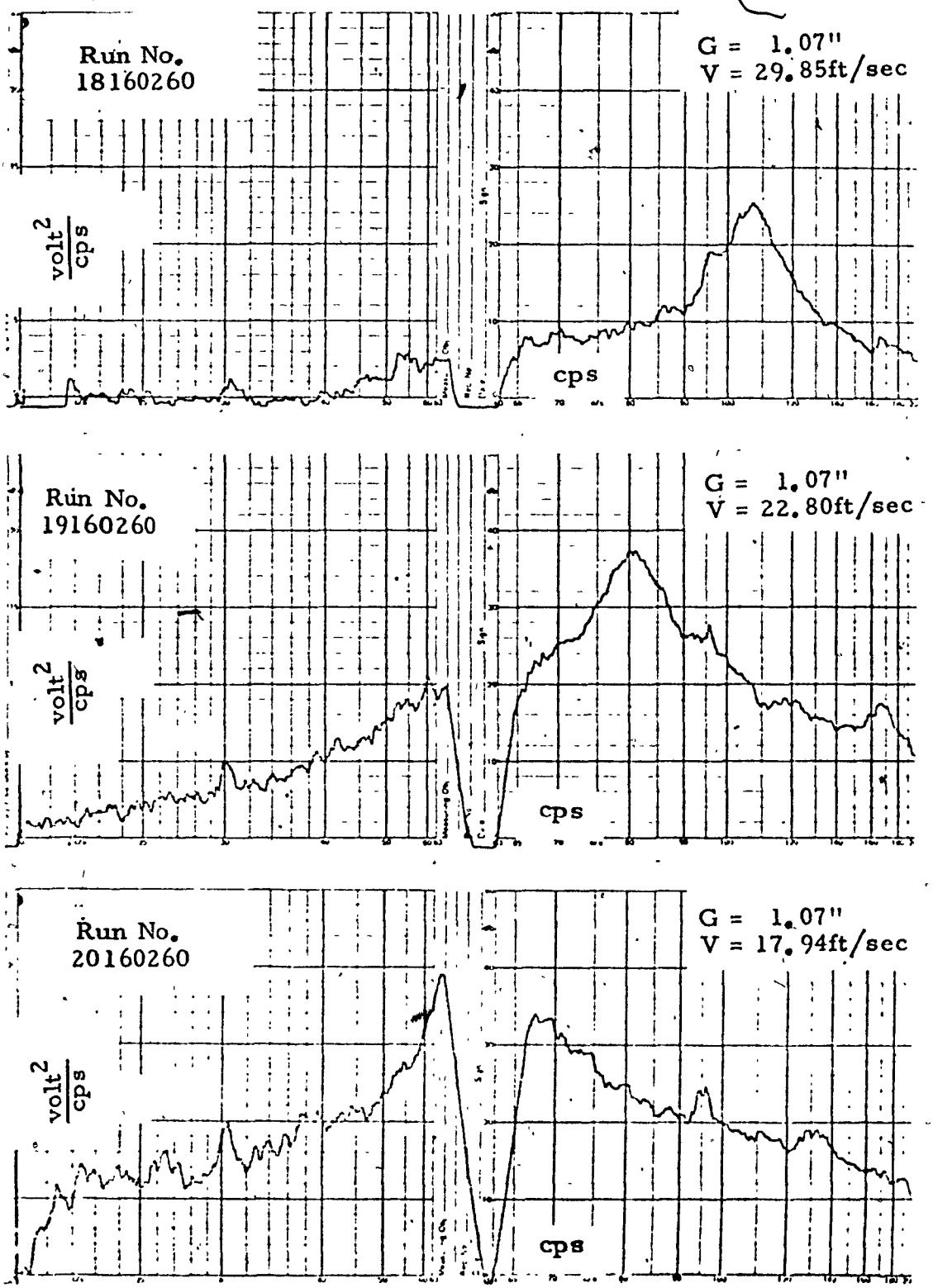
Run No.
18160260
G = 1.07"
V = 29.85ft/sec
volt²/cps
cps
Run No.
19160260
G = 1.07"
V = 22.80ft/sec
volt²/cps
cps
Run No.
20160260
G = 1.07"
V = 17.94ft/sec
volt²/cps
cps

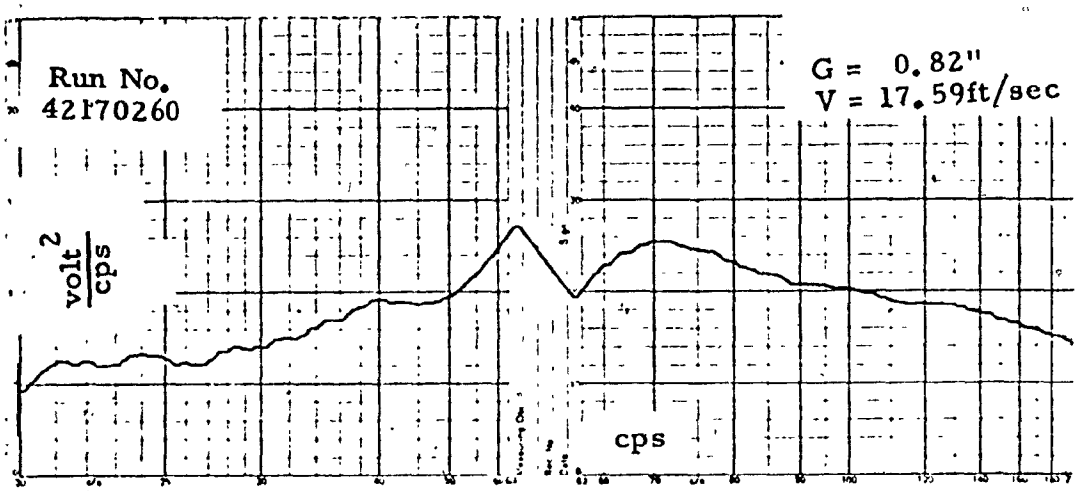
Run No.
42170260
G = 0.82"
V = 17.59ft/sec
volt²/cps
cps

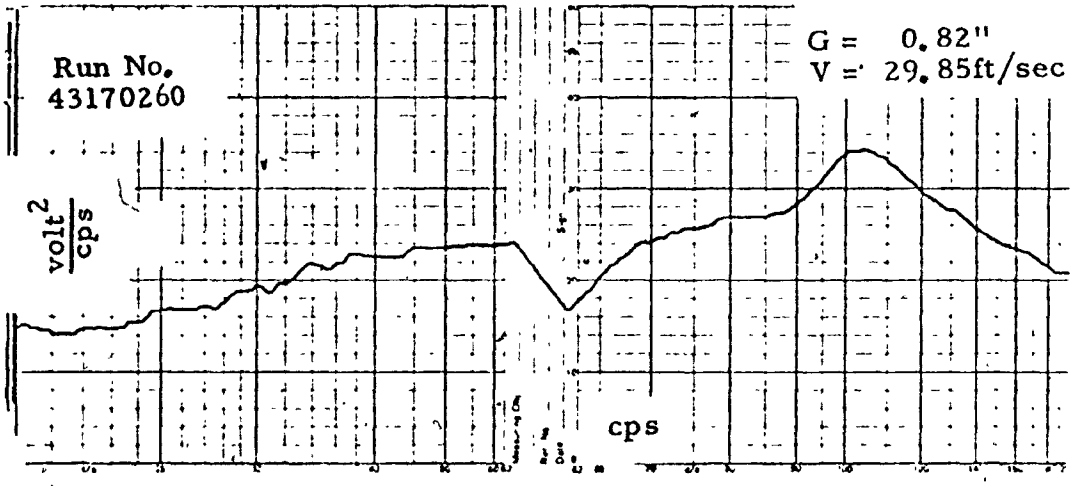
Run No.
43170260
G = 0.82"
V = 29.85ft/sec
volt²/cps
cps

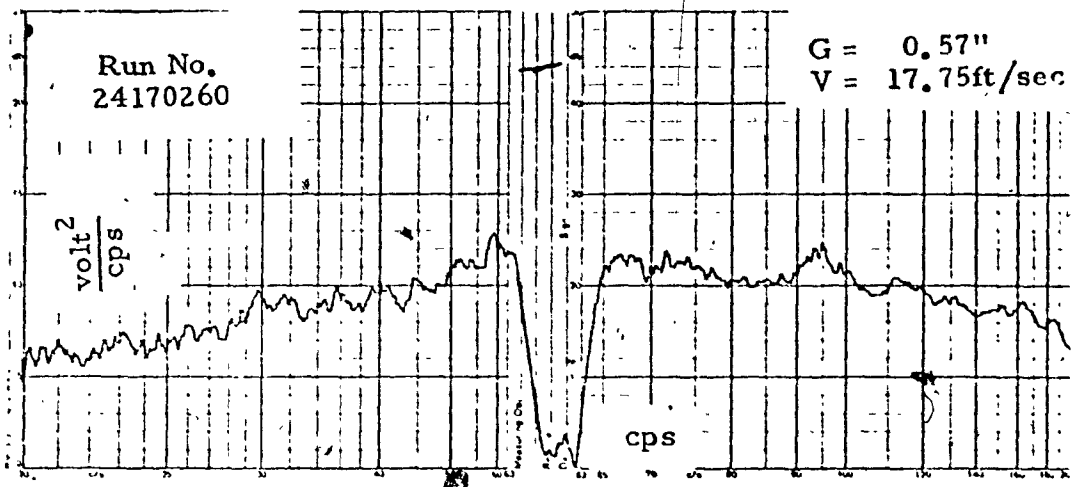
Run No.
24170260
G = 0.57"
V = 17.75ft/sec
volt²/cps
cps

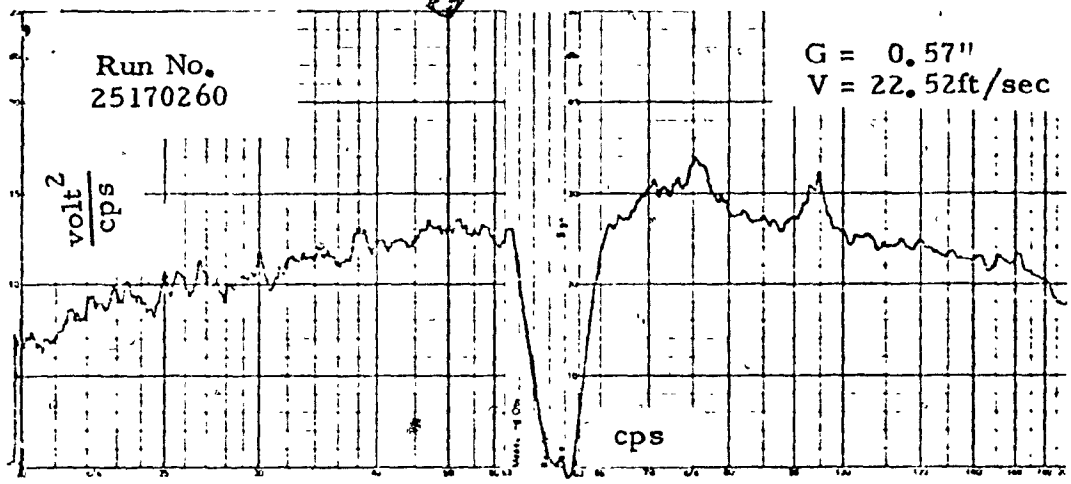
Run No.
25170260
G = 0.57"
V = 22.52ft/sec
volt²/cps
cps

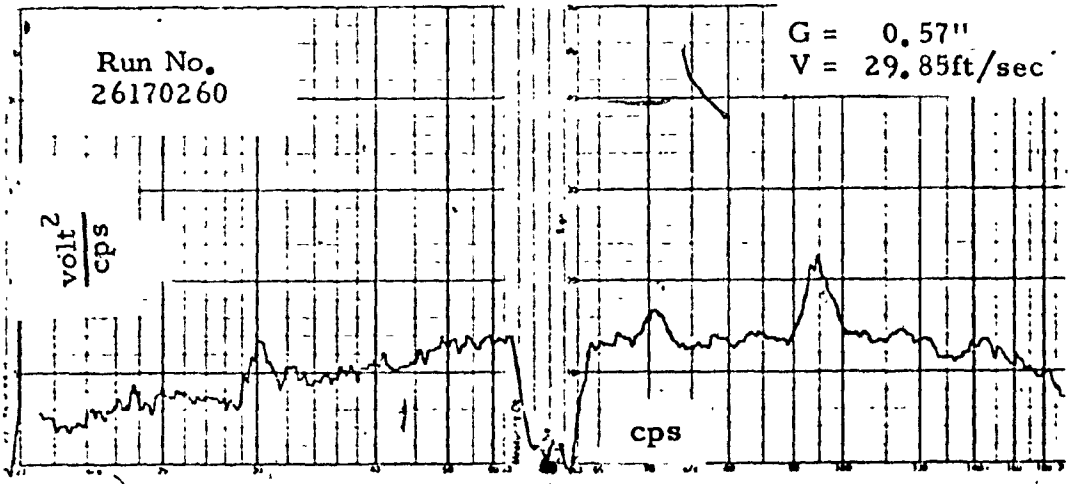
Run No.
26170260
G = 0.57"
V = 29.85ft/sec
volt²/cps
cps

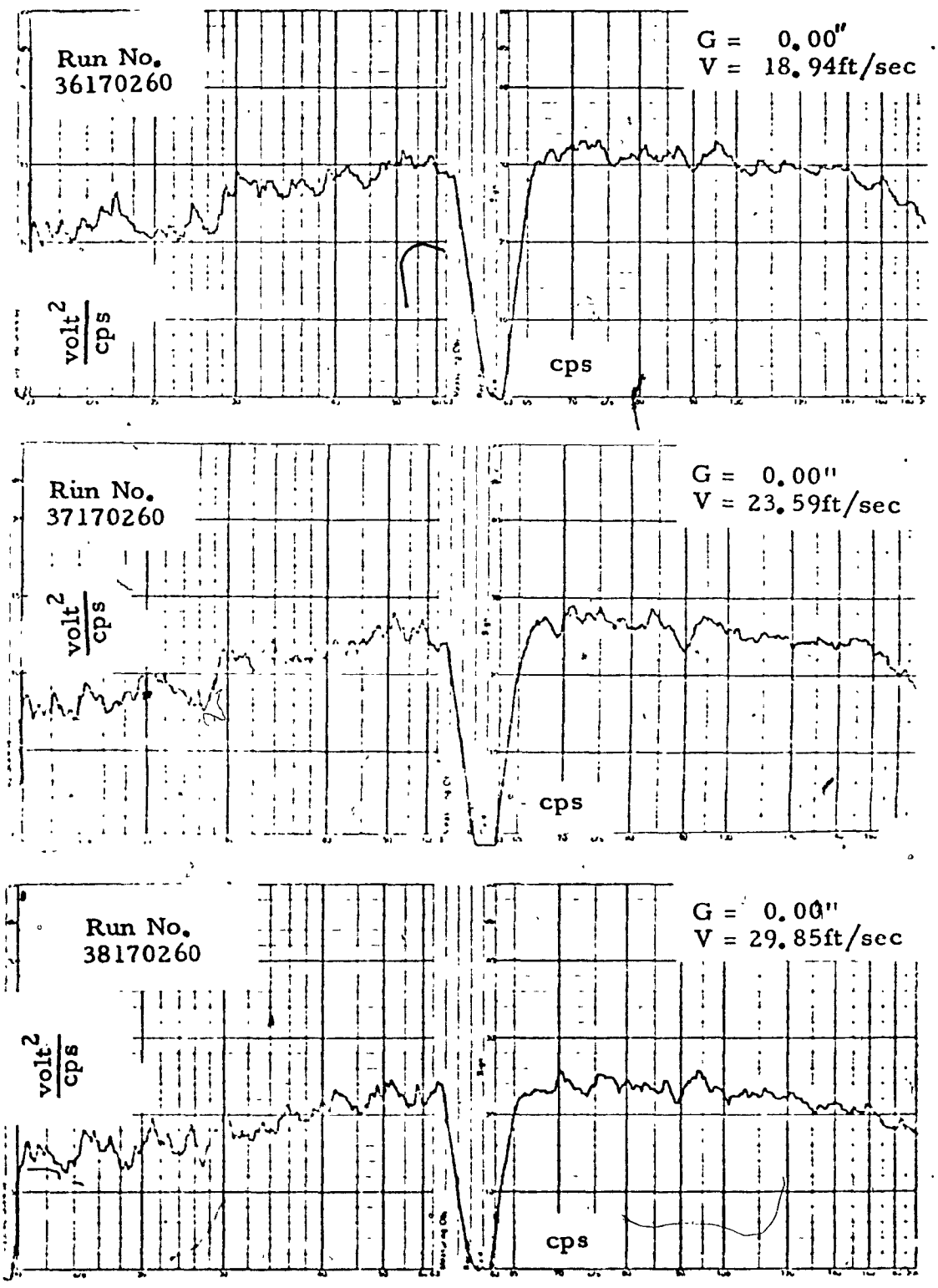
Run No.
36170260
G = 0.00"
V = 18.94ft/sec
volt²/cps
cps
Run No.
37170260
G = 0.00"
V = 23.59ft/sec
volt²/cps
cps
Run No.
38170260
G = 0.00"
V = 29.85ft/sec
volt²/cps
cps